


ORIGINAL RESEARCH

Open Access



Biochar filler in MEX and VPP additive manufacturing: characterization and reinforcement effects in polylactic acid and standard grade resin matrices

Nectarios Vidakis¹, Dimitrios Kalderis², Markos Petousis^{1*} , Emmanuel Maravelakis², Nikolaos Mountakis¹, Nikolaos Bolanakis² and Vassilis Papadakis³

Abstract

The development of sustainable and functional biocomposites remains a robust research and industrial claim. Herein, the efficiency of using eco-friendly biochar as reinforcement in Additive Manufacturing (AM) was investigated. Two AM technologies were applied, i.e., vat photopolymerization (VPP) and material extrusion (MEX). A standard-grade resin in VPP and the also eco-friendly biodegradable Polylactic Acid (PLA) in the MEX process were selected as polymeric matrices. Biochar was prepared in the study from olive trees. Composites were developed for both 3D printing processes at different biochar loadings. Samples were 3D-printed and mechanically tested after international test standards. Thermogravimetric Analysis and Raman revealed the thermal and structural characteristics of the composites. Morphological and fractographic features were derived, among others, with Scanning Electron Microscopy (SEM) and Atomic Force Microscopy (AFM). Biochar was proven to be sufficient reinforcement agent, especially in the filament MEX process, reaching more than 20% improvement at 4 wt.% loading in tensile strength compared to the pure PLA control samples. In the VPP process, results were not as satisfactory, still, a 5% improvement was achieved in the flexural strength with 0.5 wt.% biochar loading. The findings prove the strong potential of biochar-based composites in AM applications, too.

Highlights

- The reinforcement of VPP and MEX 3D printed parts with eco-friendly biochar.
- Resin and biocompatible eco-friendly PLA were the matrices.
- Eco-friendly composites achieved high-performance mechanical properties.

Keywords Biochar, Resin, Polylactic acid (PLA), Vat photopolymerization (VPP), Material extrusion (MEX), Mechanical characterization

Handling editor: Jun Meng

*Correspondence:

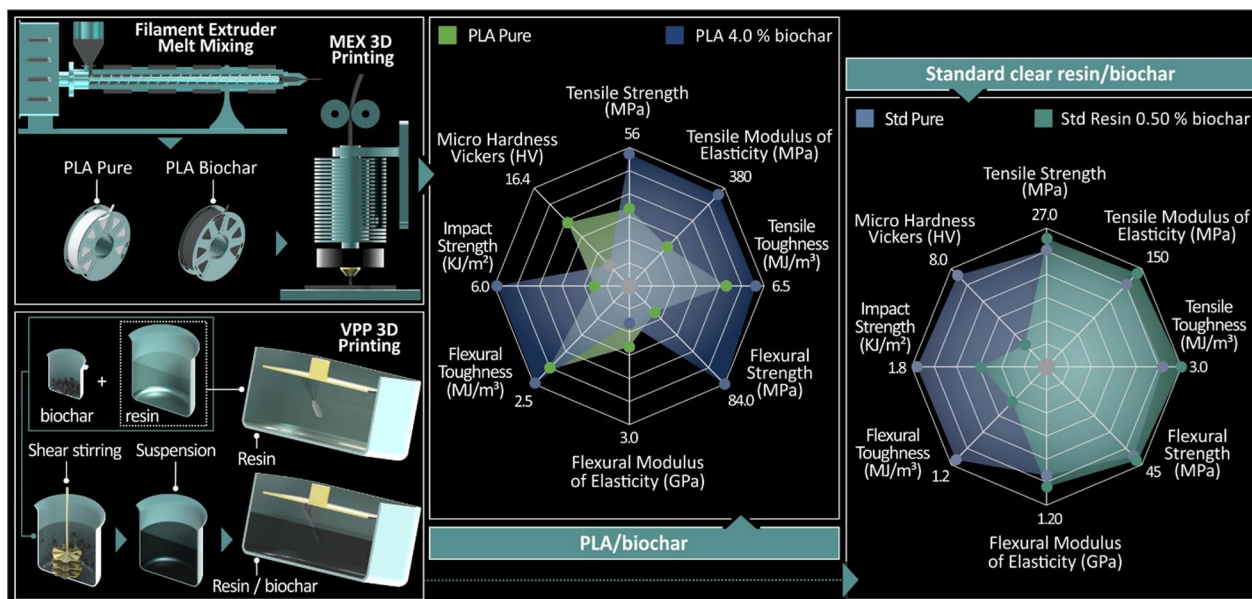
Markos Petousis
markospetousis@hmu.gr

Full list of author information is available at the end of the article



© The Author(s) 2023. **Open Access** This article is licensed under a Creative Commons Attribution 4.0 International License, which permits use, sharing, adaptation, distribution and reproduction in any medium or format, as long as you give appropriate credit to the original author(s) and the source, provide a link to the Creative Commons licence, and indicate if changes were made. The images or other third party material in this article are included in the article's Creative Commons licence, unless indicated otherwise in a credit line to the material. If material is not included in the article's Creative Commons licence and your intended use is not permitted by statutory regulation or exceeds the permitted use, you will need to obtain permission directly from the copyright holder. To view a copy of this licence, visit <http://creativecommons.org/licenses/by/4.0/>.

Graphical Abstract



1 Introduction

The development of carbon-reinforced composite materials and their application in additive manufacturing is an emerging field of research (Ghoshal 2017). Carbon derivatives, such as carbon black, carbon nanotubes, graphene, and carbon fibers have been implemented in various polymeric matrices in the material extrusion (MEX) additive manufacturing (AM) process (Acrylonitrile–butadiene–styrene–ABS (Vidakis et al. 2020), Polyamide 12–PA12 (Vidakis et al. 2023), and Polylactic Acid–PLA (Vidakis et al. 2021a) among others). The aforementioned PLA is a biocompatible, eco-friendly, and sustainable polymer (Rajeshkumar et al. 2021) with specifications that have made it popular for applications in packaging (Divakara Shetty and Shetty 2019) and in the medical field (Singhvi et al. 2019), while it is the most used polymer in MEX AM (Vidakis et al. 2022a). As expected, research on the PLA polymer has expanded to areas such as Hybrid Additive Manufacturing (HAM) to further expand its applicability, i.e., AM and laser cutting to upgrade the surface roughness and dimensional accuracy of 3D-printed workpieces (Petousis et al. 2023a), and AM combined with friction stir welding for the production of large parts (Vidakis et al. 2022c).

By varying the type of carbon, the carbon-to-matrix weight, and the resin type, the composite products exhibit improved mechanical, electrical, and thermal properties and can thus be engineered to address the

requirements of a specific application (Blyweert et al. 2021; Casamento et al. 2023). A similar positive effect has been reported by the addition of such fillers in resins in the vat photopolymerization (VPP) AM process (Peerzada et al. 2020; Yang et al. 2022; Iervolino et al. 2022). Recent examples include the application of laser metal deposition (LMD) for the development of graphene aluminum matrix composite (Li et al. 2021), the preparation of an elastic carbon nanotube/polydimethylsiloxane compressive strain sensor (Liu et al. 2022a), and the application of fused filament fabrication (FFF) for the production of a carbon fiber/polyethylene terephthalate composite (García et al. 2022). Following fabrication, these composites can be used in an increasing number of industrial processes, including the aerospace, healthcare, wind energy, and energy storage sectors (Yuan et al. 2019; Aloqalaa 2022; Dashtbozorg et al. 2022). Tamez and Taha (2021) comprehensively reviewed the use of carbon fibers in composite materials for additive manufacturing. Such composites have shown positive behavior in lightweight applications, however, there are considerable issues to be solved. These include the high initial cost of obtaining graphene or carbon fibers, the lack of control over their alignment during extrusion, and the possibility of void formation which may lead to poor mechanical properties (Tamez and Taha 2021). Furthermore, their dependence on non-renewable fossil fuels, and the complex methodologies required to obtain the final carbon

product from the raw material, largely increase their environmental footprint (Serrano-Luján et al. 2019; Yan et al. 2020; Ahmed and Mohamed 2023). Then again, the addition of metal-based fillers is a common practice to enhance the performance of resins in VPP and induce a multi-functional character on the parts built with resins with the specific AM method (Vidakis et al. 2022d). To achieve such characteristics along with an environmentally friendly profile, additives such as cellulose have been applied in VPP AM processes (Vidakis et al. 2022b). Consequently, researchers are looking for alternative, cost-efficient, and environmentally friendly approaches to obtain carbon materials suitable for additive manufacturing applications (Beloïn-Saint-Pierre and Hischer 2021).

One such material is biochar, a high-carbon, solid material obtained through the pyrolysis of residual biomass and agricultural waste. Yearly, millions of tons of unexploited biomasses are disposed of in landfills throughout the world (AliAkbari et al. 2021; Sertolli et al. 2022). As part of the circular bio-economy, many types of biomasses can be converted to added-value materials such as biochar and used in a wide range of application (Gupta et al. 2022; Tan et al. 2023). The chemical and physical attributes of biochar are strongly dependent on the pyrolysis conditions (temperature and residence time) and the properties of biomass itself (lignin, cellulose, hemicellulose, and ash content). Additionally, post-production modifications through physical and/or chemical means can adjust these properties (Goswami et al. 2022; Liu et al. 2022b; Mehdi et al. 2022). Therefore, engineered biochar can be produced according to the requirements of a specific application.

As a multi-functional material, biochar has been utilized in various application. The majority of research has focused on its beneficial role as a soil amendment due to its water and nutrient-holding capacity as well as its porous network which delivers a habitat for soil microorganisms (Adhikari et al. 2022). Other established application include its utilization as a substrate in heterogeneous catalysis (Turunç et al. 2021; Qiu et al. 2021), as an electrode for energy storage devices (Tsubota et al. 2021), as an adsorbent for the removal of organic/inorganic contaminants from water and soil (Liang et al. 2021; Qiu et al. 2022), and as a filler in cement mixtures for the development of mortars with improved properties (Danish et al. 2021). However, the use of biochar in additive manufacturing composites is limited and only a few works have demonstrated the potential of the material in this field.

The work of Idrees et al. (2018) was among the first to demonstrate the effects of adding biochar to develop a sustainable and cost-effective composite with an upgraded thermomechanical response. The authors

melt-mixed biochar with recycled PET [poly(ethylene terephthalate)] and produced 1.75 mm feedstocks using a filament extruder. The results also depicted that a 0.5% wt. loading of biochar in PET induced a 32% raise of the tensile strength, whereas a 5% wt. induction led to a 60% raise in tensile modulus compared to the raw PET matrix (Idrees et al. 2018). In a similar approach, Strongone et al. (2020) dispersed biochar from coffee waste in bisphenol-A-ethoxylate-diacrylate at various loadings in the range from 0.01 to 1.0% wt. and attempted to depict correlations between the thermal, optical, and rheological properties of the composites and the corresponding properties of the reference materials. Biochar was shown to be more readily and uniformly dispersed within the resin compared to the multi-walled carbon nanotubes (MWCNTs), thus leading to a predictable—and therefore tunable—effect on the thermal conductivity and transparency of the cured resin (Strongone et al. 2020). Interestingly, Alhelal et al. (2021) prepared biochar from the same biomass as Strongone et al. and used it as a reinforcement agent in epoxy resin to fabricate 3D printing specimens exploiting the direct-write (DW) approach with 1.0% and 3.0% wt. biochar grades. At the optimum biochar loading (1% wt.), the flexural modulus and strength of the composite reached a 55.5% and 43.4% raise, respectively. Nevertheless, increasing the 3.0% filler loading was found to have a negative impact on both the flexural and viscoelastic responses of the samples (Alhelal et al. 2021). The added value concept of sustainable waste management was referred to in the work of Mohammed et al. (2022). The authors hypothesized that biochar is not as effective as carbon nanomaterials in upgrading the thermomechanical properties of polymer materials, therefore they synthesized highly graphitized biochar from starch-derived sustainable leftovers. This modified biochar was studied as an effective reinforcement agent of polypropylene at quite small loadings between 0 and 1.0% wt. At the optimum found loading of biochar (0.75% wt.), the tensile elasticity modulus and strength experienced 34% and 46% increases, respectively (Mohammed et al. 2022). In an effort to reduce the environmental impact of the construction industry, biochar was combined with sand and cement to develop 3D printable mortars of the increased dimensional stability (Falliano et al. 2020, 2022). At biochar rates in the range of 5%–23% wt., compressive and flexural strengths higher than 60 and 8 MPa were maintained in the printed mortar, respectively, whereas up to 43% CO₂ emission reduction was achieved. The performance of biochar composites using PLA as the matrix material has also been reported. Composites have been prepared with various methods with existing

research not related to the AM processes (Arrigo et al. 2020; Aup-Ngoen and Noipitak 2020; Das et al. 2021).

On this basis, the rationale of the current investigation was to combine sustainable waste management, material science, and manufacturing processes to develop a biochar-based composite with improved mechanical and thermal properties, suitable for additive manufacturing applications. A standard-grade resin was selected as the matrix in the VPP process, whereas PLA was deployed in the MEX process for the development of an all-environmentally friendly composite with an enhanced mechanical response. To produce raw biochar, olive tree pruning was strategically selected as an abundant, renewable, and underutilized agricultural waste of the Mediterranean region. Yearly, vast quantities of this type of waste are burned in open fields to reduce their volume and eliminate the spread of diseases. However, such practice is a major organic aerosol and CO₂ source for the Mediterranean region, whereas it has a negative impact on soil structure and increases the fire risk in adjacent areas (Kostenidou et al. 2013; García Martín et al. 2020; Romero-García et al. 2022). The hypothesis is that if olive tree biochar can be used to improve the thermomechanical scores of AM polymers, then a new exploitation pathway for a major agricultural residue may be developed. VPP composites were prepared with a high-shear stirring process, while MEX composites were prepared with a thermomechanical filament extrusion process. Samples were 3D-printed with both AM processes according to the corresponding international standards for polymers' mechanical testing. Their mechanical performance was experimentally investigated. The thermal properties and compositional structure were also evaluated to verify the stability of the composites. SEM and AFM were utilized for the morphological and fractographic characterization of the samples.

Hereby, the key objectives of this research were to:

- fabricate functional biochar through cost-efficient pyrolysis of olive tree pruning residuals and evaluate it through elemental and other characterization methods,
- combine raw biochar milled powder, without any further post-production treatment, with a standard resin in the VPP AM process and PLA in the MEX AM process to produce 3D-printable composites for each AM process, and
- evaluate the thermomechanical performance and further structural and printability features of the 3D-printed composites, to quantitatively depict the potential of biochar as a natural, eco-friendly reinforcement agent in AM processes.

2 Materials and methods

2.1 Materials

2.1.1 Biochar production and characterization

Olive tree pruning biomass was locally collected (Chania, Greece). To remove impurities, the prunings were washed and then air-dried. Olive tree pruning biochar was fabricated employing flame curtain pyrolysis. The design features, materials, dimensions, and other specifications of the pyrolysis kiln utilized in the present study, are already described in an author's earlier paper (Tsubota et al. 2021). The pyrolysis reactor had a capacity of 0.5 m³.

More specifically, the prunings were divided randomly into three batches. Then flame-curtain pyrolysis was performed in triplicate. The pyrolysis of each batch lasted 1 h at a temperature of 540 ± 50 °C. The literature suggests that the variation of the temperature in this type of reactor can be very high (Jayakumar et al. 2023). To confront this issue, temperature was monitored through four thermocouples attached to 4 different spots on the external surface of the kiln. During the initial period of establishing the flame cap, considerable temperature fluctuations were observed. However, as the feeding rate of prunings (layering process) was stabilized, so did the temperature to a large extent. In flame cap pyrolysis, the uniformity of the feedstock and the optimum feeding rate is crucial to reduce the temperature fluctuations as much as possible.

After the first pruning started to pyrolyze, there was not any need for an external heating source, setting the process as self-sustained. After quenching with water, each batch of biochar was air-dried for 96 h and weighed. The 3 samples were then combined into one composite sample and homogenized. The sample was ground with the aid of a Sepor-type rod mill. After thorough sieving, the fraction of less than 100 µm in size was stored for further analyses and use. The distribution of the biochar particle size was depicted by means of a Malvern type-S Mastersizer (Malvern Instr., Malvern, UK) combined with laser diffraction. Elemental analysis (C, H, N, and S) was performed by deploying a ThermoFlash-2000 combustion analyzer (ThermoFisher Sc., UK). The content of the ash was determined after the European Biochar Certificate (EBC) Guidelines (EBC-2012, ver. 9.3E). The content of the oxygen was derived by difference. The sample chemical composition was accomplished through an X-ray fluorescence (XRF) spectrometer (Rigaku ZSX PrimuII, Japan).

2.1.2 Resin material

Resin material from the Prima company and specifically Value UV Standard Resin white color (PrimaCreator, Malmö, Sweden) was procured. The specific resin was

selected because it is affordable and high-quality. White color was selected to determine if biochar has been uniformly integrated into the resin matrix. The technical specification according to the resin datasheet is presented in Additional file 1: Table S1 in the supplementary material of the work. The composition of the resin, according to the safety data sheet of the manufacturer is presented in Additional file 1: Table S2 in the supplementary material of the work.

2.1.3 PLA polymer

The PLA used was of the 3052D grade. It was fabricated by Plastika Kritis SA (Heraklion, Crete, Greece). Its technical specifications are presented in Additional file 1: Table S3.

2.2 Methods

In the supplementary material of the work in Additional file 1: Figure S1, flow charts are presented from the experimental course followed for the preparation and characterization of the resin/biochar and the PLA/biochar compounds, along with corresponding screenshots from each step of the process.

2.2.1 Composite preparation and additive manufacturing

2.2.1.1 Preparation of resin-biochar composites and 3D printing of specimens The Phrozen Transform (Phro-

zen Technology, Hsinchu City, Taiwan, China) resin 3D printer was used to manufacture the composite samples. 3D printing started with raw material (without biochar) for the preparation of pure resin samples, which were the control samples in the study. The composites were then prepared with loadings as shown in Fig. 1. These ratios were chosen because it was not known how the resin would react to stirring with biochar (if it would be homogenized) and whether there would be a solidification of the prints with the addition of large amounts of biochar (high loadings) in the composite. For this reason, a more conservative approach to resin-biochar ratios was chosen and is the one presented below (Fig. 1). Specimens were 3D-printed at a 45° angle, and custom supports had been placed to facilitate the process. The 3D printing settings are presented in Table 1 and Fig. 1. Specimens were 3D printed with dimensions complying with the corresponding international norms (see Fig. 1) for mechanical testing. Five specimens were manufactured per test and composite.

After the 3D printing, the specimens were cleaned up with isopropyl alcohol and placed inside in a UV light oven for 5 min on each side. To create the first composite material (Resin 99.75%—Biochar 0.25%), biochar was placed into the oven to get dried for 30 min before being used. Then, it was weighed, and the resin and the biochar were placed in different mixing vessels, one for each material, and stirred for 30 min. During the

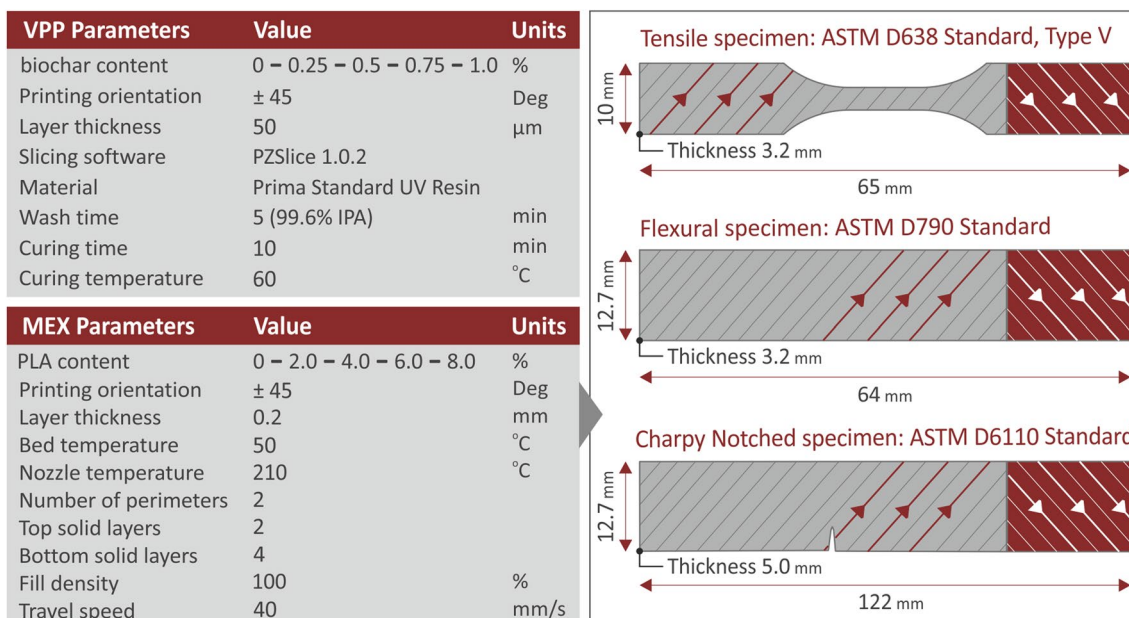


Fig. 1 MEX and VPP 3D printing settings and the biochar various loadings applied in each 3D printing process. On the right part, the geometry of the samples manufactured with the two AM methods is presented along with the corresponding international standards followed throughout the process of each mechanical test. The infill pattern used for the fabrication of the parts is also depicted in the samples

Table 1 PZSlice settings used for the specimens' 3D printing with the VPP process, on the Phrozen Transform (Phrozen Technology, Hsinchu City, Taiwan, China) resin 3D printer

Support Type	Point Size	Support Density	Support Height	Elbow Size	Bottom Size	Support Base Thickness	Base Thickness
Structure	0.5 mm	80%	6.00 mm	1.2 mm	1.5 mm	0.5 mm	1.00 mm

stirring process, the temperature of the mixture started to increase. The increase in temperature was due to the high speeds (16,000 rpm) of the stirring device. When the temperature exceeded 35 °C, the stirring was terminated to cool down the mixture for 10 min and then the stirring started again until the completion of the mixing process. By placing the resin-biochar of each mixture in the tank of the 3D printer (Phrozen Technology, Hsinchu City, Taiwan, China), the specimens of the corresponding mixture were 3D-printed. After the printing was completed, the samples were cleaned with isopropyl alcohol and inserted in the UV chamber to harden. The same process was followed for the other mixtures.

2.2.1.2 Preparation of PLA-biochar composites and 3D printing of specimens PLA-biochar composites were formed in filament for the MEX 3D printing, through a thermomechanical melt extrusion process. A two-step extrusion course was followed ensuring the scattering of the biochar in the polylactic acid matrix, to produce the composites in MEX 3D printing compatible filament form. The process is analytically presented in a former study by the authors (Petousis et al. 2023b). With the composite filament, correspondingly to the VPP method, specimens were 3D fabricated for mechanical testing. The MEX 3D printing control settings were selected in preliminary tests and in accordance with the literature for the 3D printing of the specific PLA grade (Petousis et al. 2023b) and are presented in Fig. 1 along with the biochar loading in the composite. The biochar loading was increased in the composite until processability issues in the extrusion or the 3D printing process restricted the further biochar loading increase and the mechanical properties started to decrease indicating saturation of biochar in the PLA matrix. Funmat-HT 3D printer from the Intamsys brand (Intamsys, Shanghai, China) was used for the fabrication of the test parts.

2.3 Field emission SEM and EDS

The morphological characteristics of the biochar powder and the 3D-printed parts were examined through field emission SEM (JSM-IT700HR, Jeol Ltd. Tokyo, Japan). Specimens were gold-plated whereas SEM photos were taken in a high-vacuum mode at 20 kV. The same apparatus was used for the elemental analysis of the samples

(biochar powder and 3D printed samples) by Energy Dispersive Spectroscopy (EDS).

2.4 Thermogravimetric analysis

Thermogravimetric analysis (TGA) was accomplished to gauge the thermal stability and properties of the prepared composites. A PerkinElmer Diamond (PerkinElmer, Inc., Waltham, USA) device was deployed and the process followed is analytically presented in a previous work in which the same PLA grade was studied (Petousis et al. 2022).

2.5 Raman spectroscopy

Spectroscopic analysis was accomplished by means of an adapted LabRAM-HR Raman (HORIBA Sci., Kyoto, Japan) apparatus. Analytically, the methodology followed is presented in a previous study in which the same PLA grade was studied (Petousis et al. 2022).

2.6 Atomic force spectroscopy

To evaluate quantitatively the surface topography of the VPP printed samples and the produced filament, Atomic Force Microscopy (AFM) was performed (Microscope Solver P47H-Pro device). Also, in this case, the methodology followed was presented in a previous work in which the same PLA grade was studied (Petousis et al. 2022). Surface roughness values on the measurement region were derived. Surface roughness provides a qualitative indication regarding the quality of produced filament. The filament quality is related to its processability in the MEX 3D printing process. Low-quality filaments with rough surfaces can cause issues in the MEX 3D printing process (Macedo et al. 2020).

2.7 Mechanical testing

For both the VPP and the MEX 3D fabricated samples, tensile as well as flexural tests were performed, with the aid of an ImadaMX2 (Imada Inc., Northbrook, IL, USA) device with a suitable setup for each test, complying with the relative standards (ASTM D638-14 and ASTM D790-10 respectively). Charpy notched Impact tests were performed on a Terco MT220 (Terco AB, Kungens, Sweden), following ASTM D6110, while Vickers microhardness measurements were taken according to the ASTM E384 by means of an Innova Test 400 device (Innova BV, Maas-tricht, Netherlands). Analytically the mechanical testing

methodology is presented in a previous work in which the same PLA grade was studied (Petousis et al. 2022).

3 Results

3.1 Biochar characterization

The average yield of the three runs was determined as 22% (on a dry basis), which is comparable to the yields reported for flame cap pyrolysis of woody residues (Jayakumar et al. 2023). The physicochemical characteristics of olive tree biochar are presented in Additional file 1: Table S4 in the supplementary material of the work (Nikolopoulos et al. 2023). The biochar used in this study was prepared by the current research team (Prof. D. Kalderis). The same biochar sample was used by Nikolopoulos et al. 2023. The biochar prepared herein was mechanically and manually homogenized and then characterized, therefore there was no need to perform all the characterization analyses again within the context of this study as they are reported in (Nikolopoulos et al. 2023).

The elemental content, pH, electrical conductivity, and ash content values were within the typical range of values reported earlier for woody biochars (Tu et al. 2022). The molar O/C_{org} ratio and H/C ratio indicate a high number of oxygenated functional groups on its surface (hydroxyls, phenols, ethers, carbonyls, and carboxyls), which practically means a high degree of hydrophilicity and therefore wettability of the material (Kalderis et al. 2019). However, a high concentration of oxygenated groups may lead to increased reactivity and thus degradability in the long term (Bakshi et al. 2020). Spokas (2010) portrayed the environmental constancy and stability for biochar with O/C ratios of ≤ 0.6 as highly stable (100–1000 years half-life range), whereas a C/O above 0.6 classifies biochar as rather unstable (half-life lower than 100 years). Furthermore, the O/C_{org} , H/C_{org} values and the heavy metal concentrations were well below the thresholds set by the European Biochar Certificate (EBC) for Class IV materials, which are materials that can be used in industrial application such as building composites, plastics, electronics, or textiles without risk to the environment and users (European Biochar Foundation (EBC) 2016). This is a positive first step towards the safe use of this biochar in composites. However, before a complete environmental risk assessment can be performed, the polycyclic aromatic hydrocarbon (PAHs) and dioxin content should also be determined. The BET surface area measurement was within the typical range reported for woody biochars (Tu et al. 2022).

The XRF analysis revealed a high content of CaO. The reason for the high level of CaO in biochar is the high concentration of $CaCO_3$ found in the calcareous soil the olive trees are cultivated on. Statistical analysis of the data showed that $d(0.9)$ and $d(0.5)$ values for the biochar

were 50.32 μm and 14.64 μm , respectively. Converting raw (crude) biochar to a fine powder is essential to achieve a uniform mixture with the resin at a later stage.

Figure 2C and D present two magnification images taken with SEM, of the biochar powder. The particle size was in the microscale, and they had a random wedge-type shape. Smaller and larger particles are shown in the images. Figure 2E shows the EDS graph acquired in the region shown in Fig. 2D. The elements identified were the expected ones and agreed with the XRF analysis presented above.

3.2 TGA and spectroscopic analysis of the composites

The thermal properties of the VPP and the MEX biochar composites were determined with TGA. The produced graphs (Fig. 3A, weight loss vs. temperature), show that the biochar addition did not meaningfully change the thermal response of pure materials in both the VPP and MEX process. The stability versus temperature of pure polymers was maintained through the inclusion of biochar filler, with minor differences between the curves of the composites having the same matrix material (VPP and MEX respectively). The residual mass by the completion of each measurement agreed with the biochar loading in each composite. Additionally, the composites with PLA as matrix polymer initiated measurable degradation at temperatures higher than 300 °C. This proves that the thermal setting applied to the filament melt extrusion and the 3D printing of the samples with the MEX method did not somehow affect the quality and integrity of the composites. The weight loss rate seems to slightly decrease with the addition of the biochar in both the resin and the PLA polymer. The temperature, in which the highest weight loss rate occurred was approximately the same in the resin-based composites (VPP composites). In MEX composites, the addition of biochar slightly decreased the temperature, in which the highest weight loss rate occurred, compared to the pure PLA polymer.

Figure 4 illustrates the Raman shift spectra for the resin and the PLA biochar composites. As seen in Fig. 4A the main Raman peaks arise in pure Resin. The biochar filler in resin induces insignificant differences (Table 2). As Fig. 4B shows, the major Raman peaks derive from PLA Pure. The loading of biochar in PLA specimens introduced two broad Raman curves, one between 1245⁻¹ and 1410 cm^{-1} , and the second between 1520⁻¹ and 1660 cm^{-1} . This was expected since they represent the D and G bands respectively of graphite structure in biochar as described earlier (Li et al. 2019b; Sousa et al. 2020) (Table 3). Every work cited in the following tables for the Raman spectra results has used different standards to generate the reference Raman signals and assignments. For example,

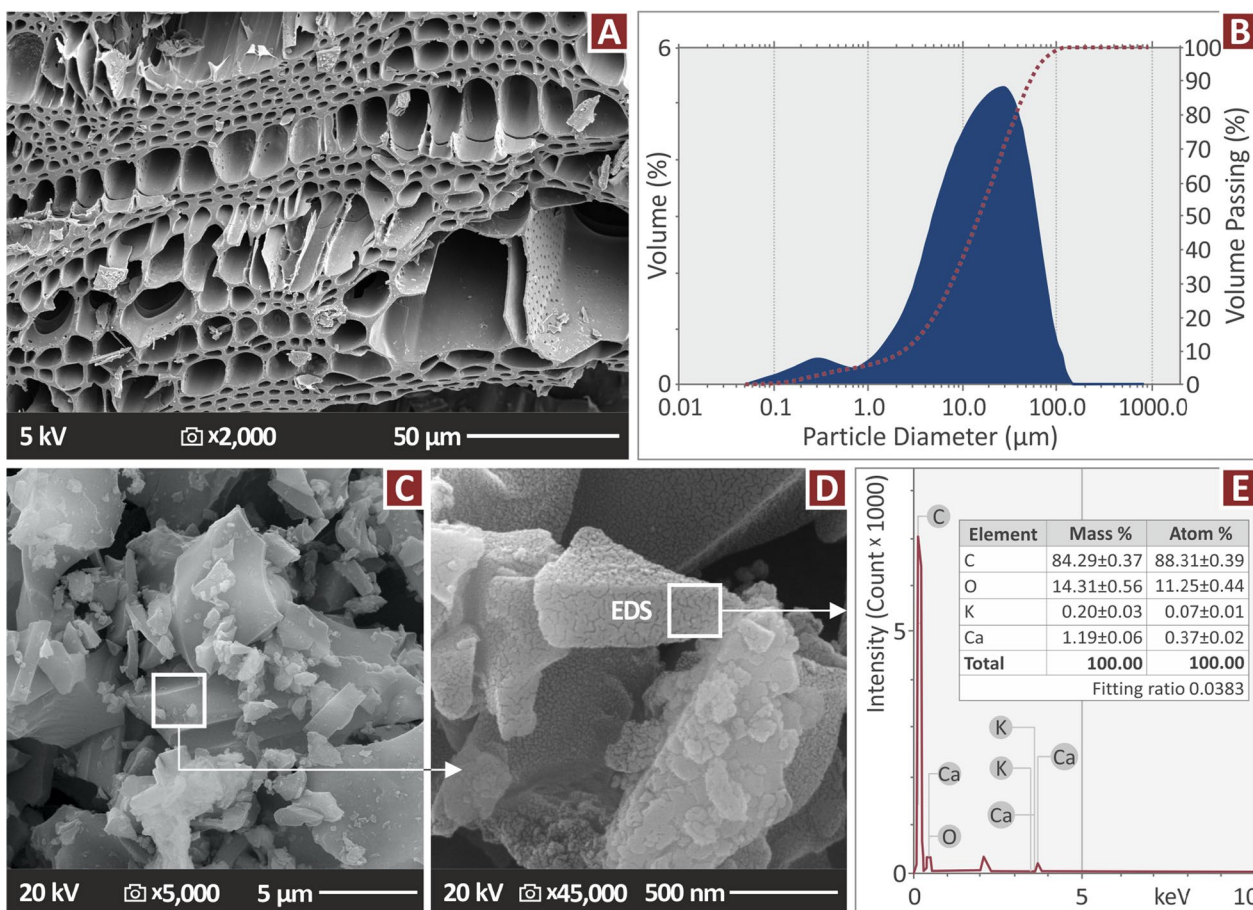


Fig. 2 Biochar morphological and compositional characterization: (A) 2000×SEM image, (B) particle size distribution, (C) 5000×SEM photo, (D) 45,000×SEM photo, (E) EDS plot depicting the elements identified in the region shown in D

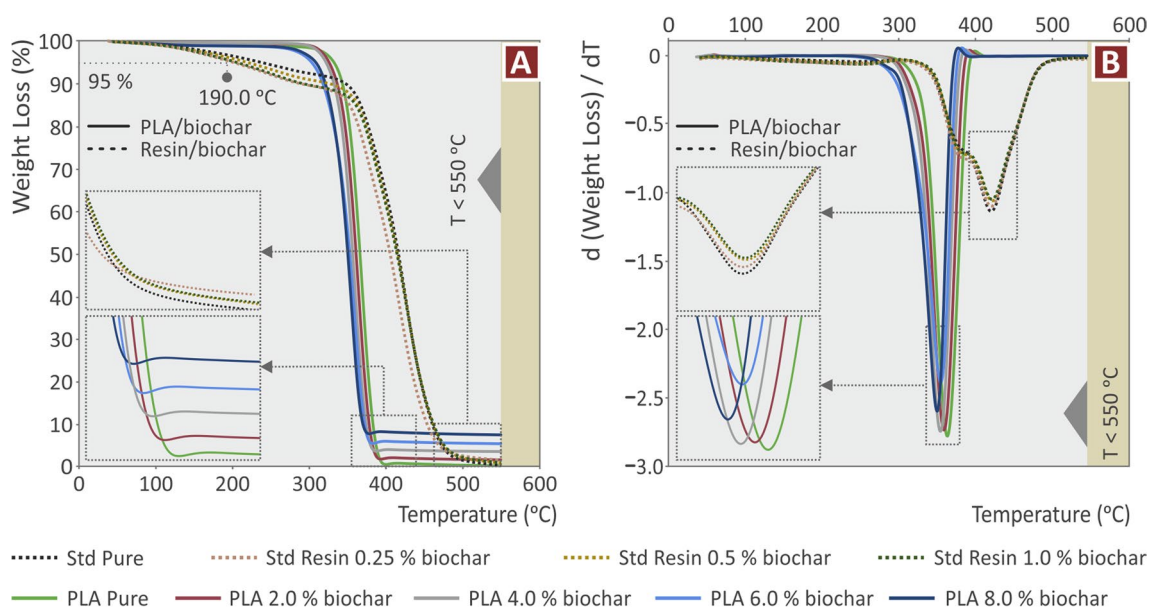


Fig. 3 Thermal response of the compounds prepared herein, derived with TGA (A) and DTGA (B) plots for VPP and MEX biochar-composites

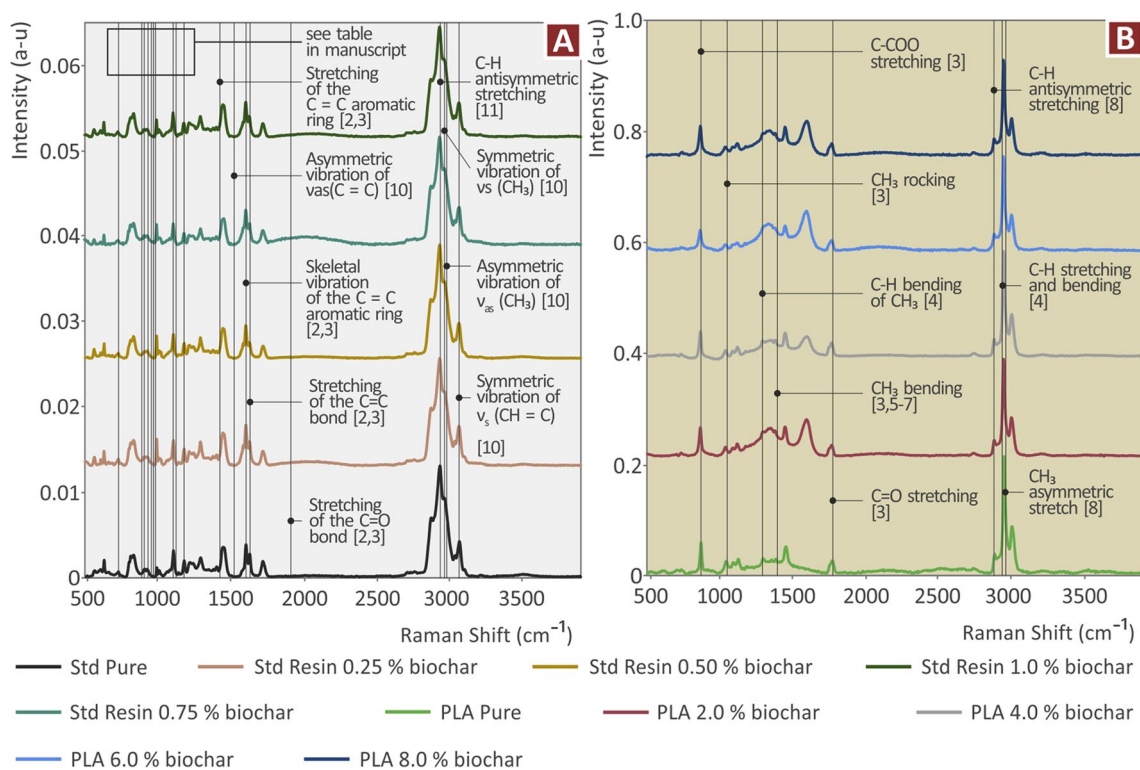


Fig. 4 Raman spectra for all samples tested, (A) Pure resin and its composites, (B) pure PLA and its composites

Table 2 Major Raman peaks identification along with their corresponding assignments for pure resin and its biochar composites

Wavenumber (cm ⁻¹)	Raman peak assignment
570	δ(COC) (Zeng et al. 2016)
812	Si–O–Si bending (Luiz et al. 2007; Gatin et al. 2022)
817	phenyl ring vibration (Stuart 1996; Zimmerer et al. 2019)
838	γ(C–OH) _{ring} (Synytsya et al. 2003; Bichara et al. 2016)
910	In-plane bending of CH ₂ (Camerlingo et al. 2007)
931	C–H bending (Stuart 1996; Resta et al. 2015)
995	γ(COOH) _{dimers} (Synytsya et al. 2003; Bichara et al. 2016)
1108	ν(C–C), ν(C–O) (Synytsya et al. 2003; Bichara et al. 2016)
1182	Methyl esters ν(COC) (Synytsya et al. 2003)
1293	Stretching of the C=O bond (Gatin et al. 2022)
1452	Stretching of the C=C aromatic ring (Luiz et al. 2007; Gatin et al. 2022)
1590	Asymmetric vibration of ν _{as} (C=C) (Montoro et al. 2014)
1607	Skeletal vibration of the C=C aromatic ring (Luiz et al. 2007; Gatin et al. 2022)
1635	C=C bond stretching (Luiz et al. 2007; Gatin et al. 2022)
1723	C=O bond stretching (Luiz et al. 2007; Gatin et al. 2022)
2873	C–H antisymmetric stretching (Liu et al. 2006)
2935	Symmetric vibration of ν _s (CH ₃) (Montoro et al. 2014)
2965	Asymmetric vibration of ν _{as} (CH ₃) (Montoro et al. 2014)
3039	Symmetric vibration of ν _s (CH=C) (Montoro et al. 2014)

Table 3 Major Raman peaks identification along with their corresponding assignments for pure PLA and the related composites with biochar

Wavenumber (cm ⁻¹)	Raman peak assignment
870	C–COO stretching (Lin et al. 2021)
1115	CH ₃ rocking (Lin et al. 2021)
1374	C–H bending of CH ₃ (Zou et al. 2009)
1449	CH ₃ bending (Stuart 1996; Resta et al. 2015; Zimmerer et al. 2019; Lin et al. 2021)
1761	C=O stretching (Lin et al. 2021)
2888	C–H antisymmetric stretching (Liu et al. 2006)
2945	C–H stretching and bending (Zou et al. 2009)
2996	CH ₃ asymmetric stretch (Liu et al. 2006)

Li et al. (2019b), have used standard phenanthrene (purity > 99%), Oxalic acid (purity > 97%), and others. The standards followed are mentioned in the corresponding literature works cited herein.

3.3 Surface morphology examination with AFM

Surface topography and roughness measurements were obtained with AFM. Roughness is a quality characteristic of composite parts. The topography of the top surface parts 3D-printed with the VPP process was examined for specimens made with the composites prepared and the measurements results are presented in Fig. 5B–E. Surprisingly, the addition of biochar reduced the surface roughness of the resin composites compared to the pure resin. No specific pattern was identified. Surface roughness was reduced at the 0.25 wt.% biochar loading and then increased with the increase of the biochar loading in the composites, but even at the resin composite with the highest biochar loading, the surface roughness was lower than that of the pure resin. Corresponding surface quality measurements were obtained on the external surface of the produced composite filament and are inserted (shaded) in Fig. 5F–I. The same trend was observed in the PLA/biochar composites, with the Ra roughness declining over the addition of biochar to the pure PLA and then increasing with the increase of the biochar loading in the composites. Again, surface roughness measurements are

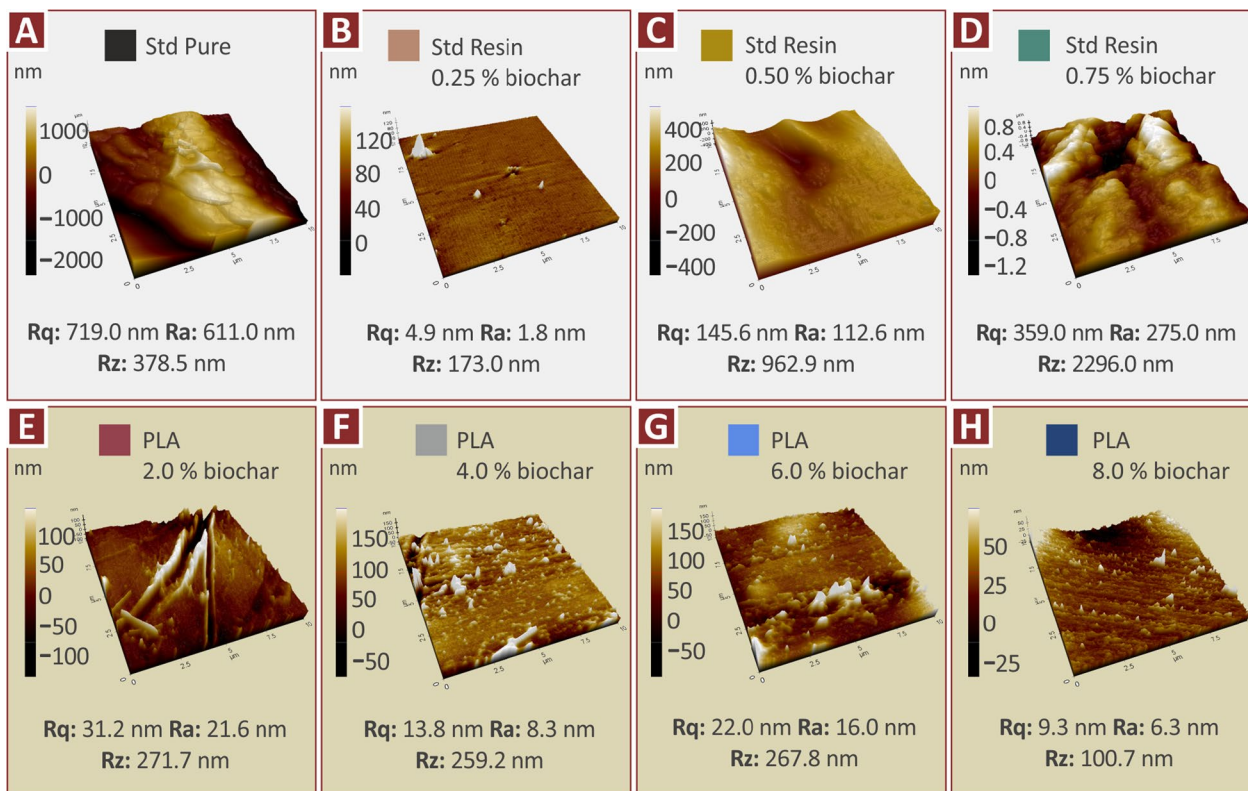


Fig. 5 Surface topography derived with AFM (A) pure resin, (B) resin/biochar 0.25 wt.%, (C) resin/biochar 0.50 wt.%, (D) resin/biochar 0.75 wt.%, and the external surface of the produced composite filament (E) PLA/biochar 2.0 wt.%, (F) PLA/biochar 4.0 wt.%, (G) PLA/biochar 6.0 wt.%, (H) PLA/biochar 8.0 wt.%

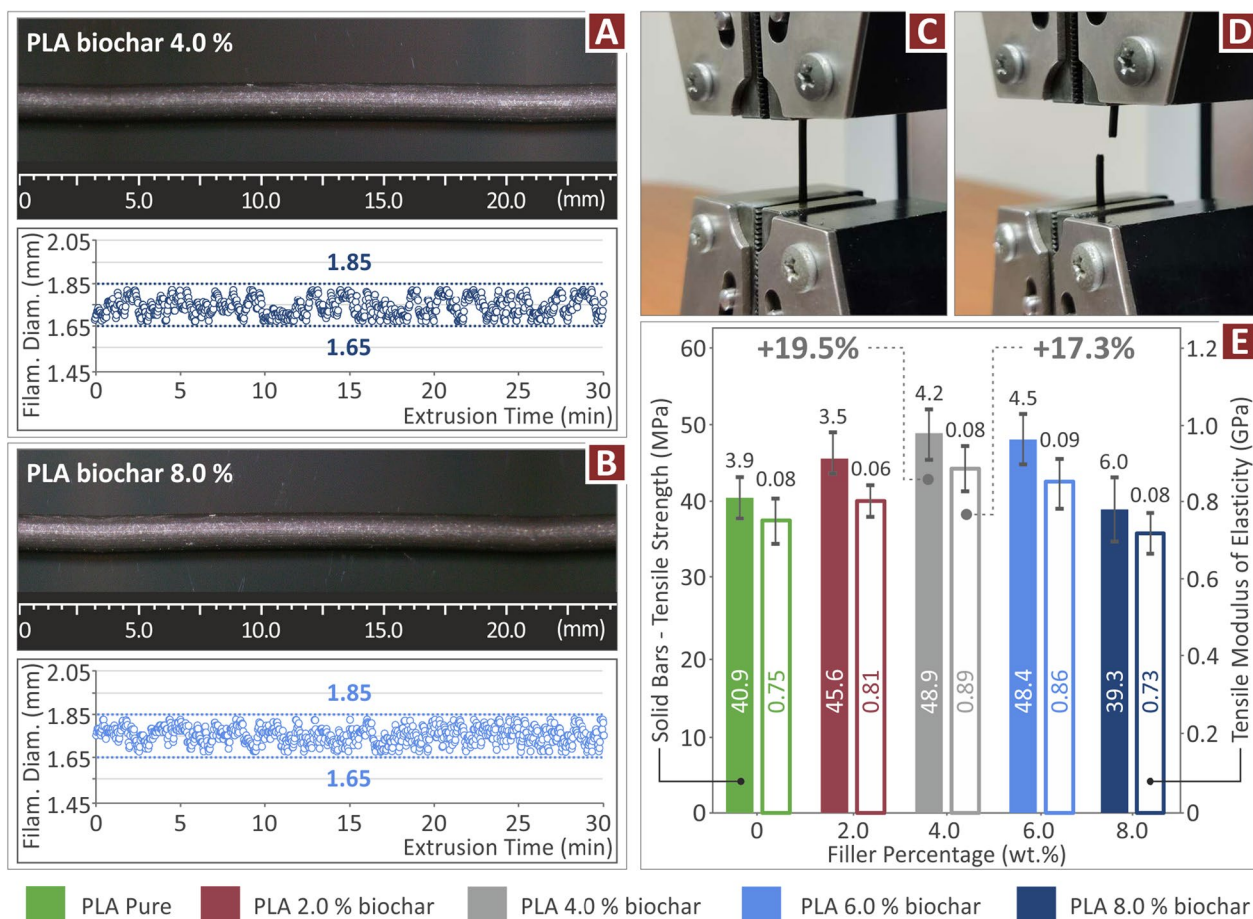


Fig. 6 Produced filament for the MEX process examination: microscopy examination and filament diameter monitoring during its extrusion course (A) PLA/biochar 4.0 wt %, (B) PLA/biochar 8.0 wt %, (C) filament tensile testing, (D) filament sample after it failed in the tensile test (E) average values of tensile strength and modulus along with their measurement deviations as they were derived from experimental procedures

lower than the pure PLA, even at the highest biochar loading composite of 8 wt.%.

3.4 MEX filament quality checks and tensile tests

The produced filament with the extrusion process for the 3D printing of the samples with the MEX method was inspected on the optical microscope (Fig. 6A and B). No defects or voids were located at the side surface, indicating a successfully completed extrusion process. During the melt extrusion course, the filament diameter was continuously monitored with a sensor embedded in a 3devo extruder. The diameter records of randomly selected periods for two different composites are shown in Fig. 6A and B, respectively. As seen, the measurements are within the same range and acceptable for the MEX 3D printing process zone, in both types of composites.

The filament was also tested for its mechanical strength in tensile tests. These tests were not performed

according to a standard procedure, still, they provided significant comparative information on the characteristics of the filament and can be correlated with the corresponding results on the 3D-printed samples. Fig. 6D depicts the tensile test results on the extruded filament for every composite prepared herein. The tensile strength and elasticity modulus are presented (average values and deviation). A clear reinforcement effect is shown in the results up to the 6 wt.% biochar loading. Beyond this point, the mechanical performance started to decline until the highest loading of 8 wt.% indicating that the saturation threshold has been reached for the biochar in the PLA matrix (marginally lower than the pure PLA at this loading, significantly reduced compared to the 6 wt.% composite). The 4 wt.% loading composite showed the highest reinforcement with a 19.5% rise in the tensile strength, as well as 17.3% in the elasticity modulus, in comparison to the pure PLA.

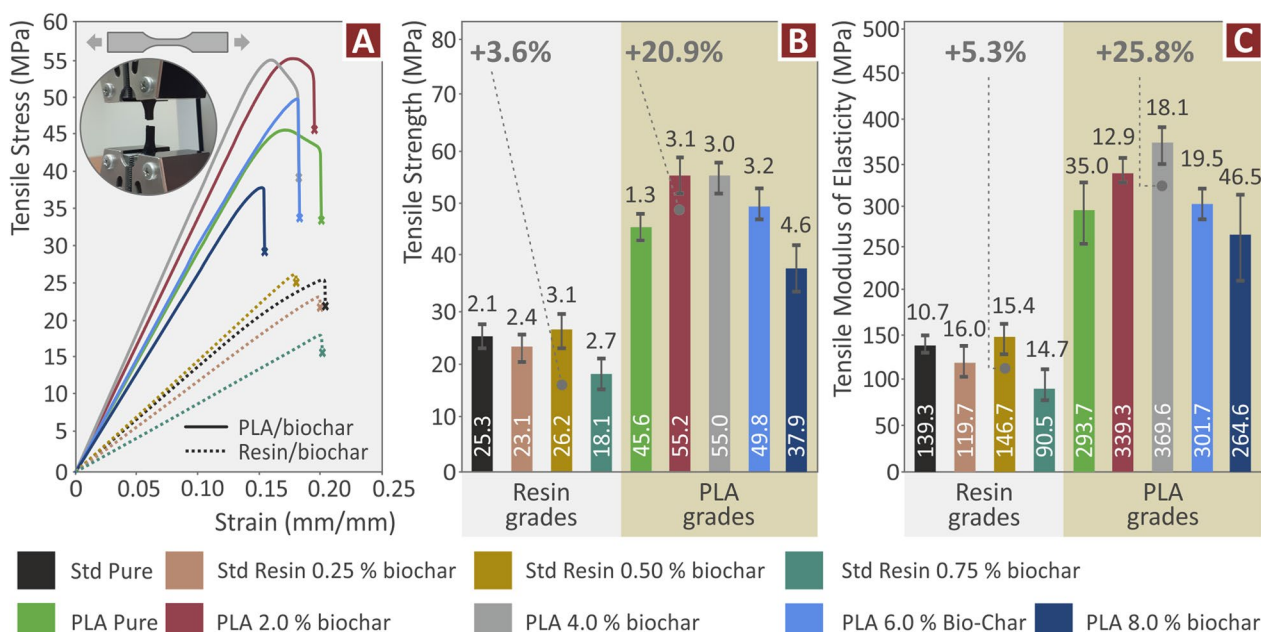


Fig. 7 Resin/biochar and PLA/biochar composites tensile test results (A) tensile stress vs. strain, (B) average tensile strength and experimental deviations, (C) average tensile modulus of elasticity and experimental deviations

3.5 Mechanical testing

The tensile test experimental results for both the resin-based and the PLA-based composites proved an evident improvement of sample strength terms, by adding biochar. In the resin/biochar composites, a 3.6% improvement was achieved in the tensile strength (Fig. 7B) and a 5.3% in the tensile elasticity modulus (Fig. 7C), through a rather low 0.50 wt.% biochar loading in the composite. In the stress vs. strain graphs (Fig. 7A), the strain was not significantly altered as a consequence of adding biochar in the resin composite, which is an indication that the ductility of the samples was not affected. This needs to be verified on the inspection with SEM that followed. The reinforcement effect on the PLA/biochar composites was more intense, probably due to the higher biochar loading in the composites. All the composites, except the one containing the maximum loading of 8 wt.% showed improved tensile properties in comparison to the PLA pure grade. The 8 wt.% biochar samples also failed at lower strain (Fig. 7A) showing that the specific loading compromised the performance of 3D-printed samples. This is an indication that the saturation threshold is between the 6.0 and 8.0 wt.% loading for the biochar additive in the PLA matrix. An increase of 20.9% to the tensile strength was achieved by the 2.0 wt.% biochar loading composite (Fig. 7B), compared to the pure control PLA, while the 4.0 wt.% loading composite achieved a 25.8% rise in the elasticity modulus (Fig. 7C). The reinforcement trend was similar to that of the filament, which

is the expected behavior. The tensile property values were higher than the respective ones for the filament. Such differences can be attributed to the fact that the filament was not tested according to a standard procedure, so the derived experimental values are not directly comparable. This is because, to the authors’ best knowledge, there is no standard available for the tensile testing of filaments. Therefore, to evaluate the mechanical performance of the produced filament and how it is affected by the biochar concentration in the composites, tensile tests were conducted using the same conditions as the 3D printed samples, which were tested according to the corresponding international standard (ASTM D638), but in the filament tests, the authors cannot claim that a standard was followed.

The flexural experimental course per sample was terminated at 5% strain, following the directives of the standard procedure (ASTM D790) (Fig. 8A). A reinforcement effect, comparable to the tensile test trend, was observed in the flexural tests. A 4.8% reinforcement in comparison to the pure control resin was reported for the 0.50 wt.% biochar loading composite. In these tests, it was not possible to 3D print a good-quality sample with the resin/biochar 0.75 wt.% composite, thus the corresponding results are missing (Fig. 8B). In the inset image, the defects of the 3D printed samples from the resin/biochar 0.75 wt.% composite can be seen. These defects are attributed to insufficient photopolymerization of the composite. The effect of carbonaceous materials in the

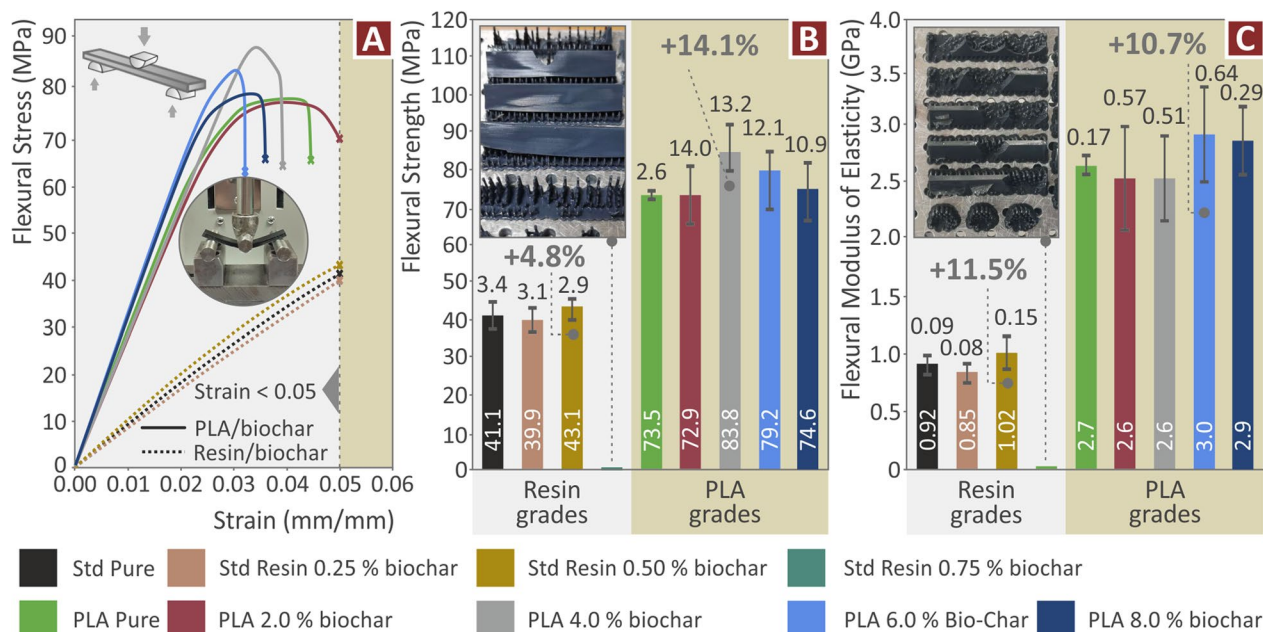


Fig. 8 Resin/biochar and PLA/biochar composites flexural test results (A) flexural stress vs. strain, (B) flexural strength findings, (C) flexural elasticity modulus findings

curing process is known and studied in the literature (Hoppe et al. 2010; Tomal et al. 2020). Thermal properties, such as enthalpy, are affected. The curing temperature is expected to be decreased with the addition of carbonaceous materials in the resins (Khan et al. 2020). Still, in the work, the curing temperature was kept at a constant value for all compounds, to have comparable results.

Regarding the PLA/biochar composites produced with the MEX process, a 14.1% rise of the flexural strength in comparison to the pure control PLA is reported for

the composite with 4.0 wt.% biochar loading, whereas a 10.7% increase in the flexural elasticity modulus for the composite with 6.0 wt.% biochar loading. At the 8 wt.% loading, the flexural properties started to decline, but still, they are marginally higher than the control PLA pure.

The toughness metric was determined as the integral of the stress over strain plots, and it shows the absorbed energy by the sample throughout the corresponding experiment. Table 4 presents the average calculated toughness and deviation per composite for the tensile

Table 4 Resin/biochar and PLA/biochar composites experimental results: average tensile toughness and deviation, average flexural toughness, and deviation, average Charpy impact strength and deviation, average Vickers microhardness and deviation

	Tensile toughness (MJ/m ³)		Flexural toughness (MJ/m ³)		Charpy impact strength (kJ/m ²)		Vickers microhardness (HV)	
	Average value	Deviation	Average value	Deviation	Average value	Deviation	Average value	Deviation
Pure Std resin	2.8	0.3	1.1	0.4	1.7	0.3	7.6	1.2
Std resin/0.25 wt.% biochar	2.2	0.4	0.4	0.2	1.1	0.5	4.5	0.5
Std resin/0.50 wt.% biochar	3.0	0.2	0.3	0.1	0.7	0.2	4.2	0.8
Std resin/0.75 wt.% biochar	1.7	0.2	-	-	-	-	4.8	1.1
PLA pure	5.3	0.2	2.3	0.2	2.4	0.4	15.9	1.1
PLA/2.0 wt.% biochar	6.5	0.8	2.5	0.2	3.6	0.8	16.0	0.5
PLA/4.0 wt.% biochar	6.2	0.3	2.5	0.2	5.8	0.9	15.3	0.7
PLA/6.0 wt.% biochar	4.7	0.2	1.6	0.1	5.5	0.4	15.7	0.7
PLA/8.0 wt.% biochar	3.2	0.6	1.9	0.1	2.9	0.8	16.3	0.3

and flexural experiments, respectively. In the tensile tests, the resin/biochar composites exhibited in general, a decreased toughness, when compared to the pure control resin. This agrees with the tensile test results and can be attributed to the deformation of the resin composites before they fail in the tensile tests. As the composites showed a less ductile behavior (reduced elongation before their failure) the area below the stress vs strain curve from which the toughness is calculated, is reduced. The toughness shows the energy absorbed by the material before it failed the tests. As the sample fails at lower strain values, the energy absorbed in the experiment is lower.

Only the 0.50 wt.% loading composite showed increased toughness by 7.3% compared to the reference samples. This was the only resin/biochar composite with increased tensile strength. The flexural toughness (Table 4) is decreased in the resin/biochar composites, in comparison to the resin pure. Furthermore, the toughness of the PLA/biochar composites followed a similar pattern to the corresponding tests, still, the biochar composites with the highest toughness values were different from those that showed the highest increase in strength in the tests. This can be attributed to a stiffer behavior (higher slope of the Hooke region) or a more ductile behavior (higher strain at failure). A 22% increase in the tensile toughness was observed for the PLA/biochar with a 2.0 wt.% biochar loading, whereas a 7% increase was determined in the flexural roughness for the PLA/biochar with 4.0 wt.% biochar loading.

The addition of biochar is reducing the impact toughness (Table 4), as well as the Vickers microhardness (Table 4) of the resin/biochar grades. On the other hand, an impressive 140% increase was achieved in the impact strength of the 4.0 wt.% loading PLA/biochar composite, compared to pure PLA. Microhardness was not influenced significantly by adding biochar in the PLA matrix, with values being similar to the pure PLA in all loadings studied. The 2.0 wt.% loading PLA/biochar composite achieved slightly higher microhardness values, increased by a marginal 0.8% compared to the pure PLA polymer.

3.6 Morphological characterization

The fractographic and morphological features of the 3D-printed samples were inspected by SEM investigations. Figure 9 presents SEM images for the resin/biochar composites. Figures 9A, D, and G present the images from the side surface of pure resin, resin/biochar 0.50 wt.%, and resin/biochar 0.75 wt.%, respectively. In the image for the pure resin, (Fig. 9A) the 3D-printed structure does not show any defects or voids. The addition of biochar in the resin matrix has a negative effect on the 3D printing structure, with minor voids visible on the sample (0.50 wt.% biochar composite, Fig. 9D). Further

increase of the biochar loading in the composite to 0.75 wt.% (Fig. 9G) significantly increased the voids that are visible on the side surface of the sample, indicating that the quality of the composite worsened. This has also a negative consequence on the mechanical performance of the parts for the highest biochar loading. Figures 9B, C, E, F, and H, and I present at two different magnifications the fracture surface of the resin/biochar grades. The fracture surface in all samples indicates a brittle fracture mechanism, as minimum deformation can be observed. The characteristic striation fans, porosity, and dimples (Ratnesh Raj et al. 2022) in the fracture surface of the VPP 3D-printed can be observed in the samples.

Figure 10 includes corresponding SEM photos for the PLA/biochar composites. The side surface of the pure PLA sample (Fig. 10A) and the PLA/biochar 4.0 wt.% (Fig. 10D) shows a defect and void-free layer fusion, with layers having a uniform and stable shape. In the sample built with PLA/biochar 8.0 wt.% composite, porosity, voids, and a non-uniform layer shape can be observed (Fig. 10G). This caused an influence on the mechanical properties of this grade case, as presented above. Figure 10B, C, E, F, H and I present at two magnification levels the fractured face of the PLA/biochar composites. Higher deformation can be observed in the pure PLA sample (Fig. 10B, and C) on the fracture surface, although the specimen overall is not significantly deformed. In the PLA/biochar 4.0 wt.% sample, the deformation in the fracture surface was minimum, still, the specimen seemed to be deformed more than the pure PLA one (change in the shape of the section is visible). Additionally, the porosity appeared to be higher in this sample than in the corresponding one made with pure PLA. Microcracks were also visible at the higher magnification image (Fig. 10F). The sample with the highest biochar loading (8 wt.%) showed the highest deformation in the shape of the specimen, although the fracture surface itself was not significantly deformed. Additionally, the porosity was increased with more pores visible and micro-pores in the fracture surface (Fig. 10H and I, respectively). The increased porosity negatively affects the mechanical performance of the 3D-printed parts (Li et al. 2019a), as was confirmed by the mechanical tests conducted. Still, such geometrical characteristics are expected in the 3D-printed structure of the parts built with the MEX process (Song et al. 2017).

4 Discussion

Herein, the potential of using an ecological, biocompatible, nature-sourced carbon-based material in powder form as a filler for enhancing the performance of pure polymeric grades used in AM, is investigated. This additive was the biochar prepared from olive tree prunings.

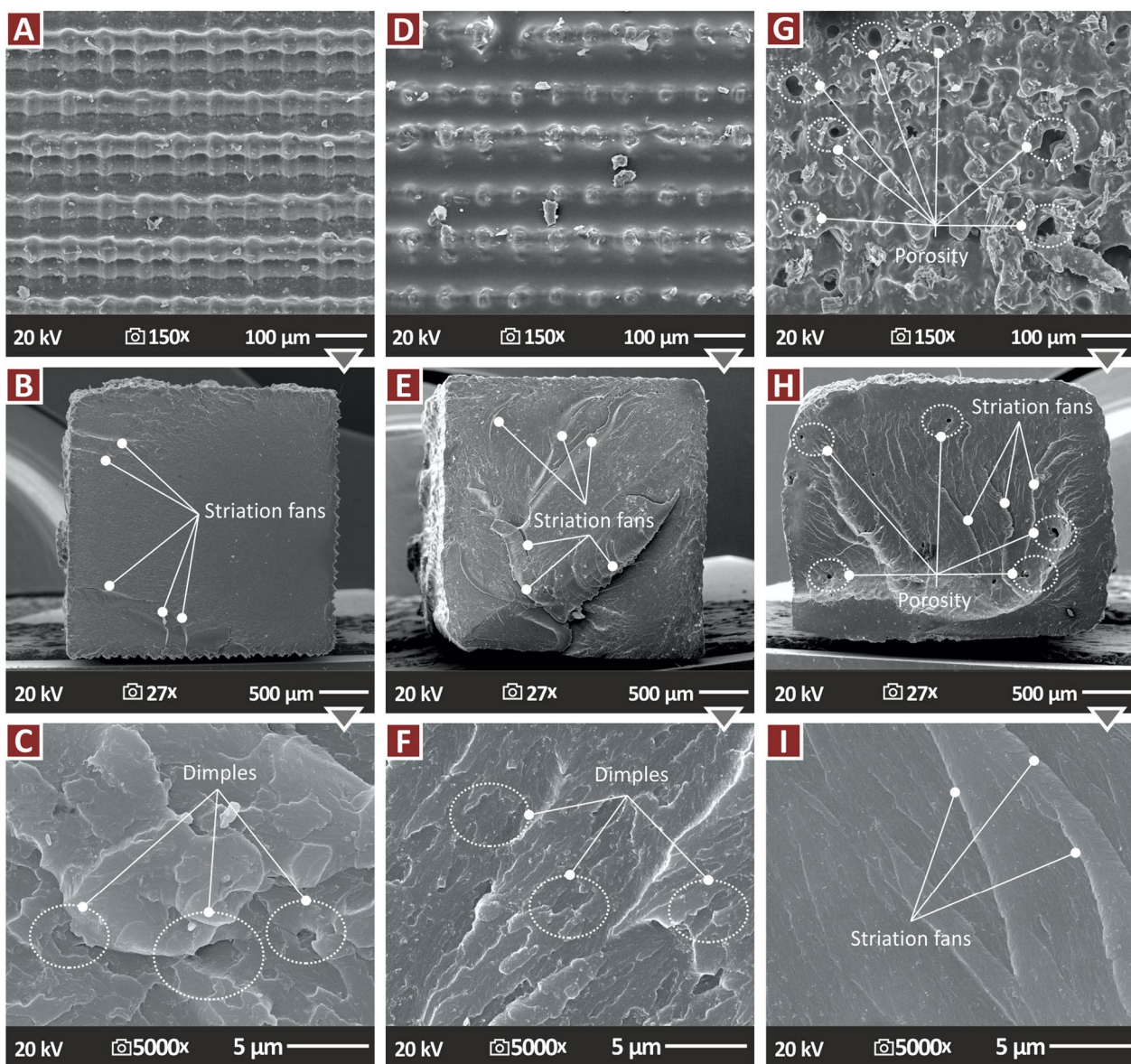


Fig. 9 SEM images taken from the resin/biochar composites. In each column are presented: top image 150 × magnification of the sample side surface, middle image 27 × magnification of the sample fractured surface, bottom image 5000 × magnification on the sample fractured surface, (A–C) pure resin, (D–F) resin/biochar 0.50 wt.%, (G–I) resin/biochar 0.75 wt.%

A standard-grade resin in VPP and PLA in MEX 3D printing was used as the matrix materials. Composites were prepared with high-shear stirring for the VPP process and with extrusion in the MEX process. From the experimental process, it was found that although biochar enhanced the performance of the resin even at low loadings (0.50 wt.%) it is not a suitable reinforcement additive, due to the processability issues that prohibited the production of higher biochar loading composites, which were expected to achieve a sufficient increase in the mechanical performance. The mechanical testing

findings are collectively plotted in radar (spider) charts provided in the supplementary material of the work for the resin/biochar composites and the PLA/biochar composites. The grey area of plots represents the pure polymers' experimental results. It is shown that only the 0.50 wt.% biochar composite had upgraded mechanical properties, in comparison to the pure control resin. On the other hand, the reinforcement effect of the biochar addition in the PLA matrix is evident, with improved mechanical response in all the tests conducted. The biochar reinforcement mechanism on polymeric materials

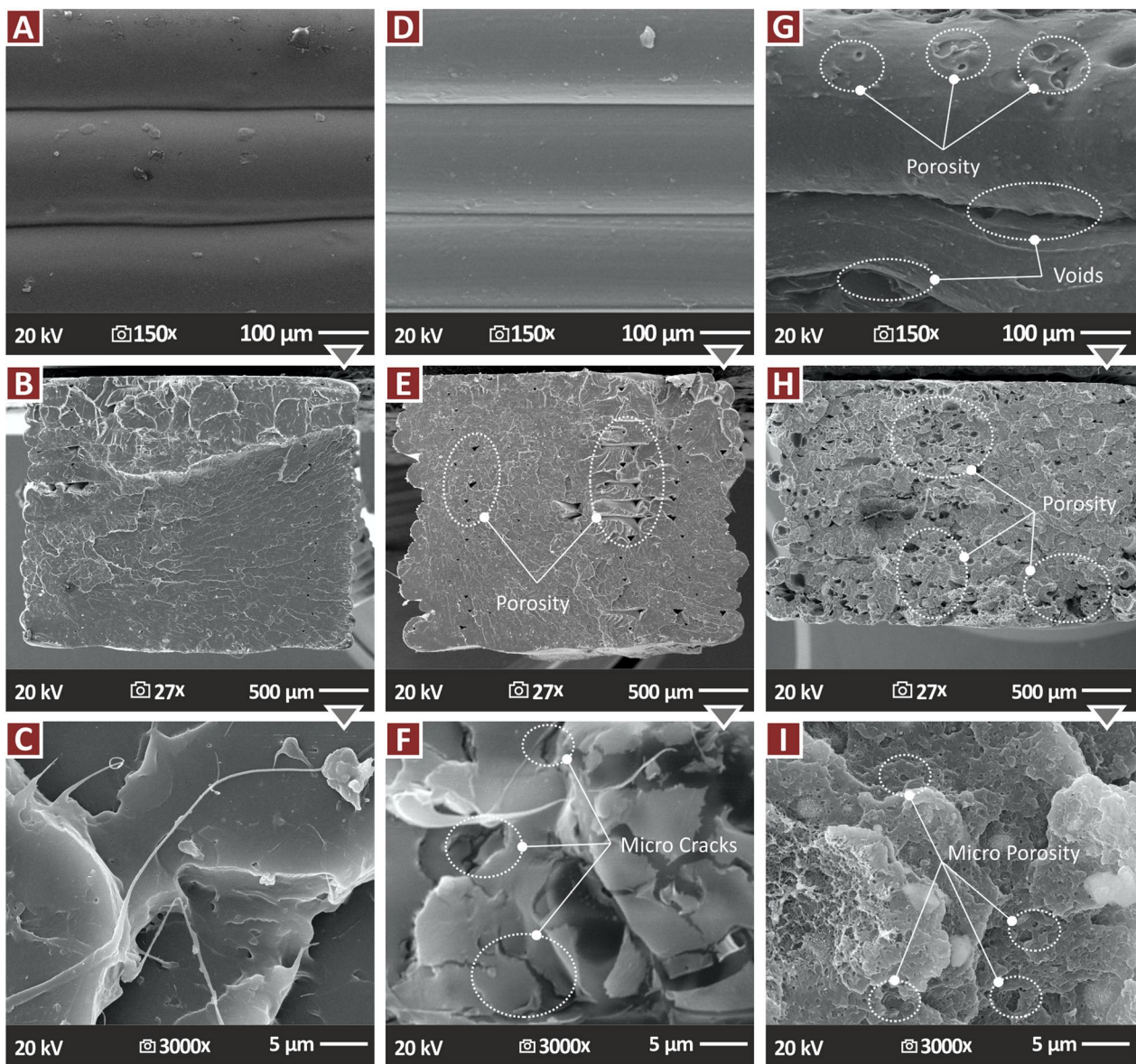


Fig. 10 SEM images taken from the PLA/biochar composites. In each column are presented: top image 150 × magnification of the sample side face, middle image 27 × magnification of the sample fractured surface, bottom image 3000 × magnification of the sample fractured surface, (A–C) pure PLA, (D–F) PLA/biochar 4.0 wt.%, (G–I) PLA/biochar 8.0 wt.%

has been investigated in the literature. It is reported that the filler structure, i.e., the aggregation structure and particle size, and the interactions on the surface between the biochar and the matrix highly affect the reinforcing mechanism of biochar (Jiang et al. 2020). The reinforcing mechanism of biochar is attributed to Vander wall interactions between the biochar and the polymer. Additionally, the reinforcing mechanism of biochar is attributed to the interlocking of polymer within micro-size pores of biochar (Mohammed et al. 2022).

In the resin/biochar composites, the increase in the tensile strength reached 3.6%, which might not be impressive, but it should be considered that this was achieved with a very low biochar loading of 0.50 wt.%. PLA/biochar composites reached a 20.9% increase in the tensile tests, with a rather low biochar loading of 2.0 wt.%, still the 4 wt.% composite had a similar response in the tensile test and improved flexural properties. So, a 4 wt.% biochar loading should be considered as the optimum loading for the PLA/biochar composite. The performance in the mechanical tests of this composite reached the

mechanical performance of high-performance polymers, such as Polycarbonate (PC) in MEX 3D printing (Vidakis et al. 2021b). This is a high-merit outcome, considering that such a performance was achieved with a composite that both the matrix and the additive materials were bio-compatible, environmentally friendly, and obtained from natural resources. In the PLA/biochar composite, in the 8 wt.% biochar loading, a saturation of the biochar in the composite occurred, as the mechanical properties were decreased. The exact saturation threshold was not identified, as it was not within the scope of the work. It should be noted that the two different composite grades were prepared with different methods, in order to produce composites compatible with each AM process (VPP and MEX) and, in both methods, reinforcement occurred.

By correlating the SEM images on the fracture surfaces (Fig. 10) and the mechanical properties found in the experiments, it can be assumed that the mechanical performance of the samples was affected by the changes in the internal structure of the parts, caused by the increase of the biochar concentrations in the composites. As shown in the SEM images of the side surface of the sample in Fig. 10, as the biochar concentration increases in the samples, the 3D printing quality is reduced, as the processability of the composites worsens. This leads to an increased number of defects in the 3D printing structure in the form of increased pores in shape and size, as shown in the fracture surface images. The reinforcing effect of biochar as the concentration increases overlaps the negative effect of the increased porosity, having an overall positive effect on the mechanical performance of the samples. Further increase of the biochar concentration leads to a 3D printing structure with an increased number of defects and reduced sample area due to the increased porosity, therefore the mechanical performance was reduced.

The findings of the current research are not directly comparable to others existing in the literature, since there is not found any similar work for the specific composites, their fabrication processes, and their feasibility and performance in AM technologies. Commercial, certified biochar derived from various natural resources, but not from olive tree prunings used herein, was introduced to resins at 2 wt.%. The preparation process was different to the one followed herein, and the biochar properties differed, and the resins investigated were different to the current study (Bartoli et al. 2019). Composites were not in a form suitable for use in the AM process. Still, the reported reinforcement effect in the work of Bartoli et al. (Bartoli et al. 2019) was rather impressive, exceeding 100% in comparison to the pure-grade resin. Differences in the performance of the composites can be attributed to the different material specifications used

in the current study, with the corresponding ones in the study of Bartoli et al. (2019), as mentioned above. In a different study, maple-derived biochar was used as reinforcement in epoxy resins with loadings of up to 20 wt.%. Composites were prepared with a different methodology than the current study and they were not compatible with the AM processes. The highest reinforcement was achieved with the 1 wt.% biochar loading composite, with an increase of about 38% compared to pure resin (Giorcelli et al. 2019a). Again, differences can be attributed to the different resin and preparation processes. Biochar has also been introduced to epoxy resins to enhance conductivity properties, due to its high carbon content (Giorcelli et al. 2019b). PLA/biochar composites have been presented in the literature, again, not in a form compatible with the AM processes, and a different preparation method was implemented. Arrigo et al. (2020) employed solvent casting and melt mixing for PLA/biochar composites development with a loading of up to 7.5 wt.%. Biochar was sourced from coffee beans. In both methods, the composites showed a stiffer response than the pure PLA, but the tensile strength was not improved with the addition of biochar. To the best knowledge of the authors, there is just one published work, which involves biochar in the MEX AM process. More specifically, biochar was derived from packaging waste, and composites were prepared from recycled Polyethylene terephthalate (PET) polymer (Idrees et al. 2018). Composites for up to 5 wt.% biochar loading was prepared and the increase in the tensile strength reached about 11% compared to the neat PET polymer (recycled without biochar additive). Differences between the results presented herein may be attributed to the dissimilar polymers studied and biochar properties. Additionally, since recycled PET was used, its exact composition was not known. Idrees et al. (2018) used peanut-shaped packaging material to produce biochar, the composition of which was very different from the olive tree prunings we used. Furthermore, they used a Ni-based superalloy high-pressure/temperature reactor, whereas herein a much simpler and cost-efficient flame pyrolysis kiln was employed. Idrees et al. (Idrees et al. 2018) combined their biochar with recycled PET, not commercial resins as the PLA used herein as the matrix material. Overall, their approach was purely from a material science point of view and did not include any environmental aspects, whereas the wider scope of the current study was not only to produce a novel composite but to develop a new valorization pathway for a major agricultural waste. Additionally, in the work recycled poly(ethylene terephthalate) was used as the matrix material, while in the current study virgin PLA was the matrix material. The biochar concentrations were similar in the two studies. In the work of Idrees, et al. tensile and

DMA tests were conducted for the evaluation of the composites' mechanical performance, while in the current study, four different tests were implemented. The work of Strongone et al. (2020) used coffee waste to produce biochar and not agricultural waste, so their biochar had very different properties. Furthermore, their pyrolysis apparatus was a commercial quartz reactor, and their biochar was produced at a much higher temperature (800 °C), compared to the process followed herein. Additionally, a different resin was the matrix material, the work focused on films and coatings, and no mechanical tests were conducted to assess the reinforcing effect of biochar, which is the main purpose of the current study. The biochar loadings on the prepared composites were similar to the ones implemented herein. Such literature investigation results verify the novelty of the current study and presented findings.

It should be noted that higher biochar concentrations on the resin matrix were not possible to be achieved. The resin/biochar suspension were not easy to prepare, and 3D print. Moreover, the addition of biochar in the resin matrix made the produced composite darker, and as the concentration increased, the photopolymerization process was not possible to be achieved. The solidification of the resin and the change of phase from liquid to solid is achieved in VPP 3D printing through the photopolymerization principle. Since this was not possible to be achieved at higher biochar concentrations, it was not possible to 3D print test samples with compounds with higher biochar concentrations with the VPP 3D printing process. So, as the biochar concentration increased, photopolymerization issues probably lead to this inferior performance of the resin/biochar composites. Carbonaceous materials absorb UV light and affect the process (Barzaegari et al. 2023). As a result, the curing time was affected (Chiu et al. 2015). In the current work, the curing time is the same in all compounds for comparison purposes. The MEX 3D printing process is based on a different operating principle (thermomechanical extrusion) and in this method higher biochar concentrations in the compounds are possible to be achieved. Regarding the Raman results, unfortunately, they do not show any significant changes in the chemistry of the specimens to explain the material strength increase. Small changes are present at 770 cm^{-1} and 781 cm^{-1} for PLA. In the STD Resin specimens, only the gradual increase of biochar is present as seen between 1245 and 1410 cm^{-1} , and between 1520 and 1660 cm^{-1} . This represents the D and G bands respectively of graphite structure in biochar. This increase is not gradual in PLA specimens.

5 Conclusions

Herein, the hypothesis of using the biocompatible, environmental-friendly biochar as reinforcement in AM polymers for two different processes, i.e., VPP and MEX was proven. This was an effort to develop biocompatible, environmental-friendly, and low-cost composites for the two most often used AM methods. A low-cost resin of standard grade was selected as the matrix in the VPP process and the biocompatible, derived from natural resources, PLA was the matrix material in the MEX 3D printing process. Biochar was collected and produced from olive tree prunings within the context of the work. Its composition and morphological characteristics were investigated and reported. The biochar addition into the two matrices did not cause any thermal instability and properties of the matrix materials. The reported structural properties were also the expected ones.

The reinforcement effect of biochar in both types of composites (resin/biochar and PLA/biochar) was found to be sufficient considering the loadings investigated, as explained above. In the VPP technique, the resin with 0.5 wt.% biochar exhibited the highest reinforcement of 3.6% in the tensile tests, while in the MEX 3D printing method the PLA with 2.0 wt.% biochar exhibited a sufficient 20.9% increase in tensile strength, compared to the unfilled PLA thermoplastic. Similar results are reported for the flexural tests as well. In the VPP 3D printing method, processability and printability issues occurred at rather low biochar loading, prohibiting the further increase of the biochar loading in the composites. This can be attributed to the specific resin grade, the VPP 3D printer used, and the known literature curing issues carbon additives induce in the composites, as explained above. Therefore, based on the current study results, it cannot be recommended as a reinforcement agent in the VPP process, at least for the specific resin. On the other hand, PLA/biochar can be considered an ecological, sustainable, and biocompatible composite with improved mechanical properties, reaching the response of high-performance polymers, as mentioned. In the MEX 3D printing method, processability issues occurred at the upper loading of 8 wt.% prepared, in which the saturation threshold for the biochar additive was exceeded. In future work, the composite preparation methods and parameters can be further optimized, in view of scaling up the process. Given the wide range of biochars and their multi-functionality, different samples should be investigated in order to determine which of their physicochemical properties play a role in the curing process and affect the properties of the composites. Such information will allow the production of engineered biochars, suitable for VPP and MEX additive manufacturing.

Supplementary Information

The online version contains supplementary material available at <https://doi.org/10.1007/s42773-023-00238-6>.

Additional file 1. An additional file is provided along with the manuscript (supplementary material), with additional information regarding the materials' properties and specifications. Additionally, the methodologies followed for the resin and the PLA composites are presented in flow chart forms and the mechanical test results are summarized in spider graph forms, one for the resin and one for the PLA composites.

Acknowledgements

Authors would like to thank the Institute of Electronic Structure and Laser of the Foundation for Research and Technology-Hellas (IESL-FORTH) and in particular Ms. Aleka Manousaki for taking the SEM images presented in this work, and the Photonic Phononic and Meta-Materials Laboratory for sharing the Raman Instrumentation. This research was partially supported by the academic fellowship of an HMU postdoctoral research program in 2022, Greece.

Author contributions

NV: Conceptualization, methodology, resources, supervision, project administration; DK: investigation, methodology, validation, formal analysis; MP: Methodology, formal analysis, writing—original draft preparation, writing—review, and editing; EM: validation, methodology; NM: data curation, visualization; NB: validation, formal analysis; VP: Visualization, Validation. The manuscript was written with the contributions of all authors. All authors have approved the final version of the manuscript.

Funding

This research received no external funding.

Availability of data and materials

The data presented in this study are available upon request from the corresponding author.

Declarations

Competing interests

The authors declare no conflict of interest.

Author details

¹Department of Mechanical Engineering, Hellenic Mediterranean University, 71410 Heraklion, Greece. ²Department of Electronic Engineering, Hellenic Mediterranean University, 73133 Chania, Greece. ³Institute of Electronic Structure and Laser of the Foundation for Research and Technology-Hellas, 71110 Heraklion, Greece.

Received: 24 March 2023 Revised: 15 June 2023 Accepted: 21 June 2023
Published online: 04 July 2023

References

- Adhikari S, Timms W, Mahmud MAP (2022) Optimising water holding capacity and hydrophobicity of biochar for soil amendment—A review. *Sci Total Environ* 851:158043. <https://doi.org/10.1016/j.scitotenv.2022.158043>
- Ahmed MA, Mohamed AA (2023) Recent progress in semiconductor/graphene photocatalysts: synthesis, photocatalytic applications, and challenges. *RSC Adv* 13:421–439. <https://doi.org/10.1039/D2RA07225D>
- Alhelal A, Mohammed Z, Jeelani S, Rangari VK (2021) 3D printing of spent coffee ground derived biochar reinforced epoxy composites. *J Compos Mater* 55:3651–3660. <https://doi.org/10.1177/00219983211002237>
- AliAkbari R, Ghasemi MH, Neekzad N, Kowsari E, Ramakrishna S, Mehrali M, Marfavi Y (2021) High value add bio-based low-carbon materials: conversion processes and circular economy. *J Clean Prod* 293:126101. <https://doi.org/10.1016/j.jclepro.2021.126101>
- Aloqalaa Z (2022) Electrically conductive fused deposition modeling filaments: current status and medical applications. *Crystals (basel)* 12:1055
- Arrigo R, Bartoli M, Malucelli G (2020) Poly (lactic Acid)—biochar biocomposites: effect of processing and filler content on rheological, thermal, and mechanical properties. *Polymers* 12:892
- Aup-Ngoen K, Noipitak M (2020) Effect of carbon-rich biochar on mechanical properties of PLA-biochar composites. *Sustain Chem Pharm* 15:100204. <https://doi.org/10.1016/j.scp.2019.100204>
- Bakshi S, Banik C, Laird DA (2020) Estimating the organic oxygen content of biochar. *Sci Rep* 10:13082. <https://doi.org/10.1038/s41598-020-69798-y>
- Bartoli M, Giorcelli M, Rosso C, Rovere M, Jagdale P, Tagliaferro A (2019) Influence of commercial biochar fillers on brittleness/ductility of epoxy resin composites. *Appl Sci (switzerland)*. <https://doi.org/10.3390/app9153109>
- Barzaegari A, Barekat M, Razavi RS, Loghman-Estarki MR, Erfanmanesh M, Razavizadeh M (2023) Effect of nanosized carbon black content on the microstructure, thermal stability, and mechanical properties of 3D printed poly urethane acrylate. *J Manuf Process* 98:113–125. <https://doi.org/10.1016/j.jmapro.2023.04.063>
- Beloin-Saint-Pierre D, Hischier R (2021) Towards a more environmentally sustainable production of graphene-based materials. *Int J Life Cycle Assess* 26:327–343. <https://doi.org/10.1007/s11367-020-01864-z>
- Bichara LC, Alvarez PE, Fiori Bimbi MV, Vaca H, Gervasi C, Brandán SA (2016) Structural and spectroscopic study of a pectin isolated from citrus peel by using FTIR and FT-Raman spectra and DFT calculations. *Infrared Phys Technol* 76:315–327. <https://doi.org/10.1016/j.infrared.2016.03.009>
- Blyweert P, Nicolas V, Fierro V, Celzard A (2021) 3D printing of carbon-based materials: a review. *Carbon NY* 183:449–485. <https://doi.org/10.1016/j.carbon.2021.07.036>
- Camerlingo C, Zenone F, Delfino I, Diano N, Mita DG, Lepore M (2007) Investigation on clarified fruit juice composition by using visible light micro-Raman spectroscopy. *Sensors* 7:2049–2061
- Casamento F, Padovano E, Pappalardo S, Frache A, Badini C (2023) Development of polypropylene-based composites through fused filament fabrication: the effect of carbon-based fillers. *Compos Part A Appl Sci Manuf* 164:107308. <https://doi.org/10.1016/j.compositesa.2022.107308>
- Chiu S-H, Wicaksono ST, Chen K-T, Chen C-Y, Pong S-H (2015) Mechanical and thermal properties of photopolymer/CB (carbon black) nanocomposite for rapid prototyping. *Rapid Prototyp J* 21:262–269. <https://doi.org/10.1108/RPJ-11-2011-0124>
- Danish A, Ali Mosaberpanah M, Usama Salim M, Ahmad N, Ahmad F, Ahmad A (2021) Reusing biochar as a filler or cement replacement material in cementitious composites: a review. *Constr Build Mater* 300:124295. <https://doi.org/10.1016/j.conbuildmat.2021.124295>
- Das C, Tamrakar S, Kiziltas A, Xie X (2021) Incorporation of biochar to improve mechanical, thermal and electrical properties of polymer composites. *Polymers (basel)* 13:1–32. <https://doi.org/10.3390/polym13162663>
- Dashtbozorg B, Tao X, Dong H (2022) Active-screen plasma surface multifunctionalisation of biopolymers and carbon-based materials—an overview. *Surf Coat Technol* 442:128188. <https://doi.org/10.1016/j.surfcoat.2022.128188>
- de Sousa DV, Guimarães LM, Félix JF, Ker JC, Schaefer CERG, Rodet MJ (2020) Dynamic of the structural alteration of biochar in ancient Anthracol over a long timescale by Raman spectroscopy. *PLoS ONE* 15:e0229447
- Divakara Shetty S, Shetty N (2019) Investigation of mechanical properties and applications of polylactic acids—a review. *Mater Res Express*. <https://doi.org/10.1088/2053-1591/ab4648>
- European Biochar Foundation (EBC) (2016) Guidelines for a Sustainable Production of Biochar. European Biochar Foundation (EBC) 1–22
- Falliano D, De Domenico D, Ricciardi G, Gugliandolo E (2020) 3D-printable lightweight foamed concrete and comparison with classical foamed concrete in terms of fresh state properties and mechanical strength. *Constr Build Mater* 254:119271. <https://doi.org/10.1016/j.conbuildmat.2020.119271>
- Falliano D, Restuccia L, Ferro GA (2022) Biochar addition for 3DCP: a preliminary study. *Procedia Struct Integrity* 41:699–703. <https://doi.org/10.1016/j.prostr.2022.05.079>
- García Martín JF, Cuevas M, Feng C-H, Álvarez Mateos P, Torres García M, Sánchez S (2020) Energetic valorisation of olive biomass: olive-tree pruning, olive stones and pomaces. *Processes* 8
- García E, Núñez PJ, Caminero MA, Chacón JM, Kamarthi S (2022) Effects of carbon fibre reinforcement on the geometric properties of PETG-based

- filament using FFF additive manufacturing. *Compos B Eng* 235:109766. <https://doi.org/10.1016/j.compositesb.2022.109766>
- Gatin E, Iordache S-M, Matei E, Luculescu C-R, Iordache A-M, Grigorescu CE, Ilici RR (2022) Raman spectroscopy as spectral tool for assessing the degree of conversion after curing of two resin-based materials used in restorative dentistry. *Diagnostics* 12:1993
- Ghoshal S (2017) Polymer/Carbon Nanotubes (CNT) nanocomposites processing using additive manufacturing (three-dimensional printing) technique: an overview. *Fibers*. <https://doi.org/10.3390/fib5040040>
- Giorcelli M, Khan A, Pugno NM, Rosso C, Tagliaferro A (2019a) Biochar as a cheap and environmental friendly filler able to improve polymer mechanical properties. *Biomass Bioenergy* 120:219–223. <https://doi.org/10.1016/j.biombioe.2018.11.036>
- Giorcelli M, Savi P, Khan A, Tagliaferro A (2019b) Analysis of biochar with different pyrolysis temperatures used as filler in epoxy resin composites. *Biomass Bioenergy* 122:466–471. <https://doi.org/10.1016/j.biombioe.2019.01.007>
- Goswami L, Kushwaha A, Kafle SR, Kim B-S (2022) Surface modification of biochar for dye removal from wastewater. *Catalysts* 12:817
- Gupta M, Savla N, Pandit C, Pandit S, Gupta PK, Pant M, Khilari S, Kumar Y, Agarwal D, Nair RR, Thomas D, Thakur VK (2022) Use of biomass-derived biochar in wastewater treatment and power production: a promising solution for a sustainable environment. *Sci Total Environ* 825:153892. <https://doi.org/10.1016/j.scitotenv.2022.153892>
- Hoppe CC, Ficek BA, Eom HS, Scranton AB (2010) Cationic photopolymerization of epoxides containing carbon black nanoparticles. *Polymer (guildf)* 51:6151–6160. <https://doi.org/10.1016/j.polymer.2010.10.057>
- Idrees M, Jeelani S, Rangari V (2018) Three-dimensional-printed sustainable biochar-recycled PET composites. *ACS Sustain Chem Eng* 6:13940–13948. <https://doi.org/10.1021/acssuschemeng.8b02283>
- Iervolino F, Bonessa A, Foti G, Levi M, Suriano R (2022) Additive manufacturing of electrically conductive nanocomposites filled with carbon nanotubes. *Adv Eng Mater* 24:2200947. <https://doi.org/10.1002/adem.202200947>
- Jayakumar A, Morrisset D, Koutsomarkos V, Wurzer C, Hadden RM, Lawton L, Edwards C, Mašek O (2023) Systematic evaluation of pyrolysis processes and biochar quality in the operation of low-cost flame curtain pyrolysis kiln for sustainable biochar production. *Curr Res Environ Sustain* 5:100213. <https://doi.org/10.1016/j.crsust.2023.100213>
- Jiang C, Bo J, Xiao X, Zhang S, Wang Z, Yan G, Wu Y, Wong C, He H (2020) Converting waste lignin into nano-biochar as a renewable substitute of carbon black for reinforcing styrene-butadiene rubber. *Waste Manag* 102:732–742. <https://doi.org/10.1016/j.wasman.2019.11.019>
- Kalderis D, Papameletiou G, Kayan B (2019) Assessment of orange peel hydrochar as a soil amendment: impact on clay soil physical properties and potential phytotoxicity. *Waste Biomass Valorization* 10:3471–3484. <https://doi.org/10.1007/s12649-018-0364-0>
- Khan TA, Gupta A, Jamari SS, Nasir M, Jang S, Kim H-J, Asim M (2020) Synthesis of micro carbonaceous material by pyrolysis of rubber wood and its effect on properties of urea-formaldehyde (UF) resin. *Int J Adhes Adhes* 99:102589. <https://doi.org/10.1016/j.ijadhadh.2020.102589>
- Kostenidou E, Kaltsonoudis C, Tsiflikiotou M, Louvaris E, Russell LM, Pandis SN (2013) Burning of olive tree branches: a major organic aerosol source in the Mediterranean. *Atmos Chem Phys* 13:8797–8811. <https://doi.org/10.5194/acp-13-8797-2013>
- Li Q, Zhao W, Li Y, Yang W, Wang G (2019a) Flexural properties and fracture behavior of CF/PEEK in orthogonal building orientation by FDM: micro-structure and mechanism. *Polymers (basel)* 11:656. <https://doi.org/10.3390/polym11040656>
- Li X, Song Y, Bian Y, Wang F, Gu C, Yang X, Jiang X (2019b) Effects of root exudates on the sorption of polycyclic aromatic hydrocarbons onto biochar. *Environ Pollut Bioavail* 31:156–165. <https://doi.org/10.1080/26395940.2019.1593054>
- Li P, Cai R, Yang G, Wang T, Han S, Zhang S, Wang W, Meng Q (2021) Mechanically strong, stiff, and yet ductile AlSi7Mg/graphene composites by laser metal deposition additive manufacturing. *Mater Sci Eng A* 823:141749. <https://doi.org/10.1016/j.msea.2021.141749>
- Liang L, Xi F, Tan W, Meng X, Hu B, Wang X (2021) Review of organic and inorganic pollutants removal by biochar and biochar-based composites. *Biochar* 3:255–281. <https://doi.org/10.1007/s42773-021-00101-6>
- Lin ZN, Guo XM, He ZP, Liang XR, Wang MM, Jin G (2021) Thermal degradation kinetics study of molten polylactide based on Raman spectroscopy. *Polym Eng Sci* 61:201–210
- Liu XB, Zou YB, Li WT, Cao GP, Chen WJ (2006) Kinetics of thermo-oxidative and thermal degradation of poly(D, L-lactide) (PDLLA) at processing temperature. *Polym Degrad Stab* 91:3259–3265
- Liu C, Le L, Zhang M, Ding J (2022a) Tunable large-scale compressive strain sensor based on carbon nanotube/polydimethylsiloxane foam composites by additive manufacturing. *Adv Eng Mater* 24:2101337. <https://doi.org/10.1002/adem.202101337>
- Liu Z, Xu Z, Xu L, Buyong F, Chay TC, Li Z, Cai Y, Hu B, Zhu Y, Wang X (2022b) Modified biochar: synthesis and mechanism for removal of environmental heavy metals. *Carbon Research* 1:8. <https://doi.org/10.1007/s44246-022-00007-3>
- Luiz BKM, Amboni RDMC, Prates LHM, Roberto Bertolino J, Pires ATN (2007) Influence of drinks on resin composite: evaluation of degree of cure and color change parameters. *Polym Test* 26:438–444. <https://doi.org/10.1016/j.polymertesting.2006.12.005>
- Macedo J, Samaro A, Vanhoorne V, Vervaeck C, Pinto JF (2020) Processability of poly(vinyl alcohol) based filaments with paracetamol prepared by hot-melt extrusion for additive manufacturing. *J Pharm Sci* 109:3636–3644. <https://doi.org/10.1016/j.xphs.2020.09.016>
- Mehdi R, Khoja AH, Naqvi SR, Gao N, Amin NA (2022) A review on production and surface modifications of biochar materials via biomass pyrolysis process for supercapacitor applications. *Catalysts* 12:798
- Mohammed Z, Jeelani S, Rangari V (2022) Effective reinforcement of engineered sustainable biochar carbon for 3D printed polypropylene biocomposites. *Composit Part C: Open Access* 7:100221. <https://doi.org/10.1016/j.jcomc.2021.100221>
- Montoro OR, Taravillo M, San Andrés M, de la Roja JM, Barrero AF, Arteaga P, Baonza VG (2014) Raman spectroscopic study of the formation of fossil resin analogues. *J Raman Spectrosc* 45:1230–1235. <https://doi.org/10.1002/jrs.4588>
- Nikolopoulos CD, Baklezos AT, Kapetanakis TN, Vardiambasis IO, Tsubota T, Kalderis D (2023) Characterization of the electromagnetic shielding effectiveness of biochar-based materials. *IEEE Access* 11:6413–6420. <https://doi.org/10.1109/ACCESS.2023.3237327>
- Peerzada M, Abbasi S, Lau KT, Hameed N (2020) Additive manufacturing of epoxy resins: materials, methods, and latest trends. *Ind Eng Chem Res* 59:6375–6390. <https://doi.org/10.1021/acs.iecr.9b06870>
- Petousis M, Vidakis N, Mountakis N, Papadakis V, Kanellou S, Gaganatsiou A, Stefanoudakis N, Kechagias J (2022) Multifunctional material extrusion 3D-printed antibacterial polylactic acid (PLA) with binary inclusions: the effect of cuprous oxide and cellulose nanofibers. *Fibers*. <https://doi.org/10.3390/fib10060052>
- Petousis M, Ninikas K, Vidakis N, Mountakis N, Kechagias D (2023a) Multifunctional PLA / CNTs nanocomposites hybrid 3D printing integrating material extrusion and CO₂ laser cutting. *J Manuf Process* 86:237–252. <https://doi.org/10.1016/j.jmapro.2022.12.060>
- Petousis M, Vidakis N, Mountakis N, Moutsopoulou A, Papadakis VM, Maravelakis E (2023b) On the substantial mechanical reinforcement of Polylactic Acid with Titanium Nitride ceramic nanofillers in material extrusion 3D printing. *Ceram Int*. <https://doi.org/10.1016/j.ceramint.2023.02.001>
- Qiu M, Hu B, Chen Z, Yang H, Zhuang L, Wang X (2021) Challenges of organic pollutant photocatalysis by biochar-based catalysts. *Biochar* 3. <https://doi.org/10.1007/s42773-021-00098-y>
- Qiu M, Liu L, Ling Q, Cai Y, Yu S, Wang S, Fu D, Hu B, Wang X (2022) Biochar for the removal of contaminants from soil and water: a review. *Biochar* 4:19. <https://doi.org/10.1007/s42773-022-00146-1>
- Raj R, Dixit AR, Singh SS, Paul S (2022) Print parameter optimization and mechanical deformation analysis of alumina-nanoparticle doped photocurable nanocomposites fabricated using vat-photopolymerization based additive technology. *Addit Manuf*. <https://doi.org/10.1016/j.addma.2022.103201>
- Rajeshkumar G, Arvinth Seshadri S, Devnani GL, Sanjay MR, Siengchin S, Prakash Maran J, Al-Dhabi NA, Karuppiah P, Mariadhas VA, Sivarajasekar N, Ronaldo Anuf A (2021) Environment friendly, renewable and sustainable poly lactic acid (PLA) based natural fiber reinforced composites—a comprehensive review. *J Clean Prod* 310:127483. <https://doi.org/10.1016/j.jclepro.2021.127483>

- Resta V, Quarta G, Lomascolo M, Maruccio L, Calcagnile L (2015) Raman and Photoluminescence spectroscopy of polycarbonate matrices irradiated with different energy 2Si^+ ions. *Vacuum* 116:82–89. <https://doi.org/10.1016/j.vacuum.2015.03.005>
- Romero-García JM, López-Linares JC, del Contreras M, Romero I, Castro E (2022) Exploitation of olive tree pruning biomass through hydrothermal pretreatments. *Ind Crops Prod* 176:114425. <https://doi.org/10.1016/j.indcrop.2021.114425>
- Serrano-Luján L, Víctor-Román S, Toledo C, Sanahuja-Parejo O, Mansour AE, Abad J, Amassian A, Benito AM, Maser WK, Urbina A (2019) Environmental impact of the production of graphene oxide and reduced graphene oxide. *SN Appl Sci* 1:179. <https://doi.org/10.1007/s42452-019-0193-1>
- Sertoli A, Gabnai Z, Lengyel P, Bai A (2022) Biomass potential and utilization in worldwide research trends— a bibliometric analysis. *Sustainability* 14
- Singhvi MS, Zinjarde SS, Gokhale DV (2019) Poly(lactic acid): synthesis and biomedical applications. *J Appl Microbiol* 127:1612–1626. <https://doi.org/10.1111/jam.14290>
- Song Y, Li Y, Song W, Yee K, Lee K-YY, Tagarielli VL (2017) Measurements of the mechanical response of unidirectional 3D-printed PLA. *Mater Des* 123:154–164. <https://doi.org/10.1016/j.matdes.2017.03.051>
- Spokas KA (2010) Review of the stability of biochar in soils: predictability of O: C molar ratios. *Carbon Manag* 1:289–303. <https://doi.org/10.4155/cmt.10.32>
- Strongone V, Bartoli M, Jagdale P, Arrigo R, Tagliaferro A, Malucelli G (2020) Preparation and characterization of UV-LED curable acrylic films containing biochar and/or multiwalled carbon nanotubes: effect of the filler loading on the rheological, thermal and optical properties. *POLYCK* 12
- Stuart BH (1996) Temperature studies of polycarbonate using Fourier transform Raman spectroscopy. *Polym Bull* 36:341–346. <https://doi.org/10.1007/BF00319235>
- Synysya A, Čopíková J, Matějka P, Machovič V (2003) Fourier transform Raman and infrared spectroscopy of pectins. *Carbohydr Polym* 54:97–106. [https://doi.org/10.1016/S0144-8617\(03\)00158-9](https://doi.org/10.1016/S0144-8617(03)00158-9)
- Tamez MBA, Taha I (2021) A review of additive manufacturing technologies and markets for thermosetting resins and their potential for carbon fiber integration. *Addit Manuf* 37:101748. <https://doi.org/10.1016/j.addma.2020.101748>
- Tan S, Zhou G, Yang Q, Ge S, Liu J, Cheng YW, Yek PNY, Wan Mahari WA, Kong SH, Chang J-S, Sonne C, Chong WWF, Lam SS (2023) Utilization of current pyrolysis technology to convert biomass and manure waste into biochar for soil remediation: a review. *Sci Total Environ* 864:160990. <https://doi.org/10.1016/j.scitotenv.2022.160990>
- Tomal W, Chachaj-Brekiesz A, Popielarz R, Ortyl J (2020) Multifunctional biphenyl derivatives as photosensitizers in various types of photopolymerization processes, including IPN formation, 3D printing of photocurable multiwalled carbon nanotubes (MWCNTs) fluorescent composites. *RSC Adv* 10:32162–32182. <https://doi.org/10.1039/d0ra04146g>
- Tsubota T, Tsuchiya S, Kusumoto T, Kalderis D (2021) Assessment of biochar produced by flame-curtain pyrolysis as a precursor for the development of an efficient electric double-layer capacitor. *Energies (base)* 14:7671
- Tu P, Zhang G, Wei G, Li J, Li Y, Deng L, Yuan H (2022) Influence of pyrolysis temperature on the physicochemical properties of biochars obtained from herbaceous and woody plants. *Bioresour Bioprocess* 9:131. <https://doi.org/10.1186/s40643-022-00618-z>
- Turunç E, Akay S, Baran T, Kalderis D, Tsubota T, Kayan B (2021) An easily fabricated palladium nanocatalyst on magnetic biochar for Suzuki-Miyaura and aryl halide cyanation reactions. *New J Chem* 45:12519–12527. <https://doi.org/10.1039/D1NJ00941A>
- Vidakis N, Maniadi A, Petousis M, Vamvakaki M, Kenanakis G, Koudoumas E (2020) Mechanical and electrical properties investigation of 3D-printed acrylonitrile–butadiene–styrene graphene and carbon nanocomposites. *J Mater Eng Perform* 29:1909–1918. <https://doi.org/10.1007/s11665-020-04689-x>
- Vidakis N, Petousis M, Kourinou M, Velidakis E, Mountakis N, Fischer-Griffiths PE, Grammatikos S, Tzounis L (2021a) Additive manufacturing of multifunctional poly(lactic acid) (PLA)—multiwalled carbon nanotubes (MWCNTs) nanocomposites. *Nanocomposites* 7:184–199. <https://doi.org/10.1080/20550324.2021.2000231>
- Vidakis N, Petousis M, Velidakis E, Spiridakis M, Kechagias JD (2021b) Mechanical performance of fused filament fabricated and 3d-printed polycarbonate polymer and polycarbonate/ cellulose nanofiber nanocomposites. *Fibers* 9:74. <https://doi.org/10.3390/fib9110074>
- Vidakis N, David C, Petousis M, Sagris D, Mountakis N, Moutsopoulou A (2022a) The effect of six key process control parameters on the surface roughness, dimensional accuracy, and porosity in material extrusion 3D printing of polylactic acid: prediction models and optimization supported by robust design analysis. *Adv Ind Manuf Eng* 5:100104. <https://doi.org/10.1016/j.aime.2022.100104>
- Vidakis N, Petousis M, Michailidis N, Kechagias JD, Mountakis N, Argyros A, Boura O, Grammatikos S (2022b) High-performance medical-grade resin radically reinforced with cellulose nanofibers for 3D printing. *J Mech Behav Biomed Mater* 134:105408. <https://doi.org/10.1016/j.jmbbm.2022.105408>
- Vidakis N, Petousis M, Mountakis N, Kechagias JD (2022c) Material extrusion 3D printing and friction stir welding: an insight into the weldability of polylactic acid plates based on a full factorial design. *Int J Adv Manuf Technol* 121:3817–3839. <https://doi.org/10.1007/s00170-022-09595-1>
- Vidakis N, Petousis M, Papadakis VM, Mountakis N (2022d) Multifunctional medical grade resin with enhanced mechanical and antibacterial properties: the effect of copper nano-inclusions in vat polymerization (VPP) additive manufacturing. *J Funct Biomater*. <https://doi.org/10.3390/jfb13040258>
- Vidakis N, Petousis M, Velidakis E, Mountakis N, Grammatikos SA, Tzounis L (2023) Multi-functional medical grade Polyamide12/Carbon Black nanocomposites in material extrusion 3D printing. *Compos Struct*. <https://doi.org/10.1016/j.compstruct.2023.116788>
- Yan Y, Nashath FZ, Chen S, Manickam S, Lim SS, Zhao H, Lester E, Wu T, Pang CH (2020) Synthesis of graphene: potential carbon precursors and approaches. *Nanotechnol Rev* 9:1284–1314. <https://doi.org/10.1515/ntrev-2020-0100>
- Yang L, Zheng D, Jin G, Yang G (2022) Fabrication and formability of continuous carbon fiber reinforced resin matrix composites using additive manufacturing. *Crystals (base)* 12:649
- Yuan S, Shen F, Chua CK, Zhou K (2019) Polymeric composites for powder-based additive manufacturing: materials and applications. *Prog Polym Sci* 91:141–168. <https://doi.org/10.1016/j.progpolymsci.2018.11.001>
- Zeng Y, Yarbrough JM, Mittal A, Tucker MP, Vinzant TB, Decker SR, Himmel ME (2016) In situ label-free imaging of hemicellulose in plant cell walls using stimulated Raman scattering microscopy. *Biotechnol Biofuels* 9:256. <https://doi.org/10.1186/s13068-016-0669-9>
- Zimmerer C, Matulaitiene I, Niaura G, Reuter U, Janke A, Boldt R, Sablinskas V, Steiner G (2019) Nondestructive characterization of the polycarbonate—octadecylamine interface by surface enhanced Raman spectroscopy. *Polym Test* 73:152–158. <https://doi.org/10.1016/j.polymertesting.2018.11.023>
- Zou HT, Yi CH, Wang LX, Liu HT, Xu WL (2009) Thermal degradation of poly(lactic acid) measured by thermogravimetry coupled to Fourier transform infrared spectroscopy. *J Therm Anal Calorim* 97:929–935

Submit your manuscript to a SpringerOpen® journal and benefit from:

- Convenient online submission
- Rigorous peer review
- Open access: articles freely available online
- High visibility within the field
- Retaining the copyright to your article

Submit your next manuscript at ► [springeropen.com](https://www.springeropen.com)